

# The subducted oceanic crust within continental-type UHP metamorphic belt in the North Qaidam, NW China: Evidence from petrology, geochemistry and geochronology

Guibin Zhang<sup>a</sup>, Shuguang Song<sup>a</sup>, Lifei Zhang<sup>a,\*</sup>, Yaoling Niu<sup>b</sup>

<sup>a</sup> MOE Key Laboratory of Orogenic Belts and Crustal Evolution, School of Earth and Space Sciences, Peking University, Beijing 100871, China

<sup>b</sup> Department of Earth Science, Durham University, Durham, DH1 3LE, UK

Received 28 April 2007; accepted 6 December 2007

Available online 23 December 2007

---

## Abstract

Three types of eclogite, together with a serpentinized harzburgite, coexist as blocks within granitic and pelitic gneisses along the Shaliuhe cross section, the eastern part of the North Qaidam continental-type ultrahigh-pressure (UHP) metamorphic belt, NW China. The olivine (Ol<sup>1</sup>) and orthopyroxene in the harzburgite are compositionally similar to present-day abyssal peridotites. The kyanite–eclogite is derived from a troctolitic protolith, whereas the epidote–eclogite from a gabbroic protolith, both having distinct positive Eu anomalies, low TiO<sub>2</sub>, and high Al<sub>2</sub>O<sub>3</sub> and MgO. The kyanite–eclogite shows inherited cumulate layering. The phengite–eclogite has high TiO<sub>2</sub>, low Al<sub>2</sub>O<sub>3</sub> and MgO with incompatible trace elements resembling enriched-type MORB. Sr–Nd isotope data indicate that the protoliths of both kyanite–eclogite and epidote–eclogite ( $[^{87}\text{Sr}/^{86}\text{Sr}]_i \sim 0.703\text{--}0.704$ ;  $\varepsilon_{\text{Nd}}(T) \sim 5.9\text{--}8.0$ ) are of mantle origin (e.g., ocean crust signatures). On the other hand, while the lower  $\varepsilon_{\text{Nd}}(T)$  value (1.4–4.1) of phengite–eclogite is more or less consistent with an enriched MORB protolith, their high  $[^{87}\text{Sr}/^{86}\text{Sr}]_i$  ratio (0.705–0.716) points to an additional enrichment in their history, probably in a subduction-zone environment. Field relations and geochemical analyses suggest that the serpentinized harzburgite and the three types of eclogite constitute the oceanic lithological section of an ophiolitic sequence from mantle peridotite, to cumulate, and to upper basaltic rocks. The presence of coesite pseudomorphs and quartz exsolution in omphacite plus thermobarometric calculations suggests that the eclogites have undergone ultrahigh pressure metamorphism (i.e., peak  $P \geq 2.7$  GPa). The harzburgite may also have experienced the same metamorphism, but the lack of garnet suggests that the pressure conditions of  $\leq 3.0$  GPa. Zircon U–Pb SHRIMP dating shows that the eclogites have a protolith age of  $516 \pm 8$  Ma and a metamorphic age of  $445 \pm 7$  Ma. These data indicate the presence of a Paleo-Qilian Ocean between Qaidam and Qilian blocks before the early Ordovician. The ophiolitic assemblage may be the relics of subducted oceanic crust prior to the subduction of continental materials during Ordovician–Silurian times and ultimate continent collision. These rocks, altogether, record a complete history of ocean crust subduction, to continental subduction, and to continental collision.

© 2007 Elsevier B.V. All rights reserved.

**Keywords:** Eclogite; Harzburgite; Geochemistry; SHRIMP dating of zircon; Oceanic subduction; North Qaidam, NW China

---

## 1. Introduction

High Pressure and Ultra-High Pressure metamorphic rocks in orogenic belts record geodynamic histories of lithospheric subduction and exhumation. Pacific-type (or B-type) and Alpine-type (or A-type) orogenic belts have been coined (Maruyama et al., 1996; Ernst, 1988, 2001) to describe scenarios of oceanic and continental lithosphere subduction/exhumation respectively (Song et al., 2006). Oceanic subduction/exhumation

zones are characterized by ophiolite mélange, island arc assemblages, and Low Temperature/High Pressure metamorphic rock suites (e.g. North Qilian, West Tianshan, China), whereas continental subduction/exhumation zones are dominated by granitic gneisses, metasediments with minor eclogites and ultramafic rocks of HP and UHP origin (e.g. Dabie–Sulu, China; West Gneiss Region, Norway). The North Qaidam UHP belt is a type continental subduction/exhumation zone comprising paragneisses, eclogites and garnet peridotites with coesite (Yang et al., 2001; Song et al., 2003a) and diamond (Song et al., 2005b) found as inclusions in zircons. In contrast to eclogite from continental UHP belts elsewhere (e.g. Dabie–Sulu, West Gneiss

---

\* Corresponding author.

E-mail address: [Lfzhang@pku.edu.cn](mailto:Lfzhang@pku.edu.cn) (L. Zhang).

Region), eclogites from the North Qaidam belt are geochemically of ocean crustal protoliths (Song, 2001; Song et al., 2003b; Meng et al., 2003; Yang et al., 2003; Song et al., 2006). Therefore, whether there indeed existed oceanic subduction in the history of the Qaidam UHP continental belt is crucial for understanding the evolution of the plate tectonic convergence from oceanic lithosphere subduction, to continental subduction, and collision.

In this paper, we report a petrologic, geochemical and geochronological study of the Shaliuhe eclogite–gneiss terrane located at the eastern part of the North Qaidam UHP belt. We identified three types of eclogite and associated serpentinized

harzburgite, representing a snapshot of subduction-zone metamorphism of oceanic lithosphere before the closure of the Paleo-Qilian ocean basin.

## 2. Geological setting

The North Qaidam UHP belt is the eastern part of the North Qaidam–Altun super-belt, which extends NWW–SEE for ~1000 km offset by the sinistral Altyn Tagh fault at the northern margin of the Tibetan Plateau (Fig. 1a). The Altun HP/UHP rocks are the western equivalent beyond the Altyn Tagh fault (Liu et al.,

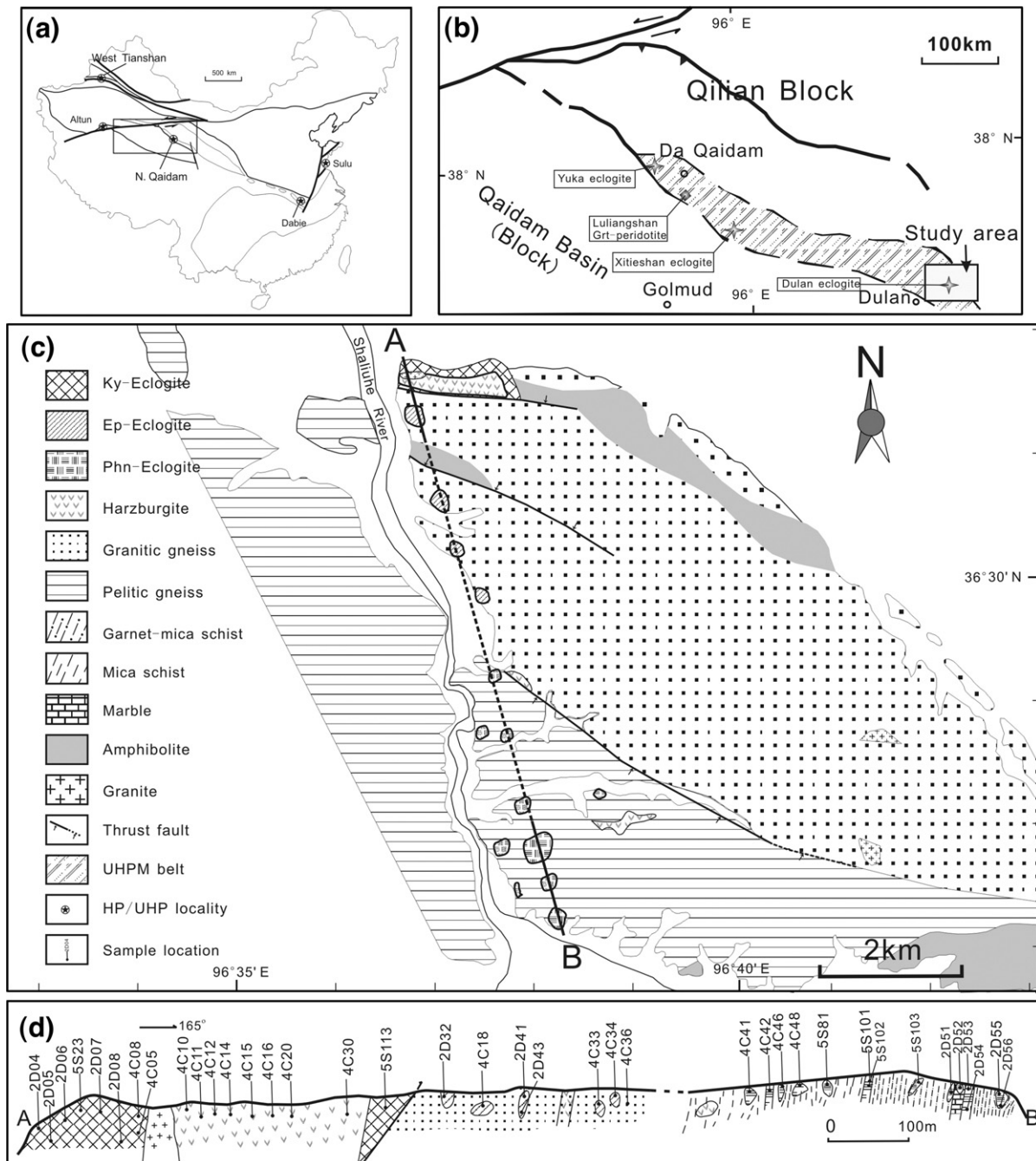


Fig. 1. Geological sketch map showing the locality of North Qaidam in China (a), distribution of UHP rocks in the North Qaidam UHP metamorphic belt (b), Shaliuhe UHP metamorphic terrane (c) (line AB: locality of cross section), a representative cross section (d) (the dashed segment means the abbreviatory part).

1999; Zhang et al., 2001; 2005b; Mattinson et al., 2007). The North Qaidam UHP belt proper lies between the Qaidam Block (south) and the Qilian Block (north), extending from Yuka southeastward through Xitieshan to Dulan for about 400 km long (Fig. 1b). A large block of garnet peridotite–pyroxenite, which crops out in the Luliangshan area (Fig. 1b) of the belt (Yang and Deng, 1994), is exhumed convincingly from depths in excess of 200 km (Song et al., 2004, 2005a,b).

The Qaidam Block to the south is a Mesozoic intracontinental basin developed on the Precambrian basement. The Qilian Block to the north mainly comprises Paleozoic sedimentary rocks underlain by an imbricate thrust belt of Precambrian basement. The North Qaidam UHP belt is interpreted as resulting from the subduction of the Qaidam block beneath the Qilian block during the closure of the Paleo-Qilian Ocean Basin in the Paleozoic (Yang et al., 2001; Song et al., 2003b, 2006).

The North Qaidam UHP metamorphism shows clear age variations. U/Pb dating of metamorphic zircons from Yuka eclogites yields 488–495 Ma (Menold et al., 2002; Zhang et al., 2005b). Xitieshan eclogites give a similar UHP metamorphic age of

~486 Ma (Zhang et al., 2005b). Song et al. (2003b, 2006) obtained ~460 Ma age by Sm–Nd isochron and Zircon U–Pb dating for eclogite, and ~420 Ma age by Zircon U–Pb dating for coesite-bearing gneisses from the Dulan area. So, a ~40 m.y. gap was proposed between eclogite formation and UHP metamorphism of pelitic gneiss (Song et al., 2006). On the other hand, Mattinson et al. (2006) suggested a ~25 m.y. duration (422–449 Ma) of eclogite-facies metamorphism for Dulan eclogite. Nevertheless, the UHP metamorphism appears to become younger towards east.

The location of this current study is in the Shaliuhe area situated at the eastern end of the Dulan UHPM Terrane, where eclogites, granitic and pelitic gneisses, serpentized harzburgites and marbles coexist (Fig. 1c). For this study, we collected samples systematically along a ~10 km long traverse (the A–B cross section in Fig. 1c and d). On the basis of mineral assemblage, three types of eclogite can be recognized, i.e., kyanite (Ky)–eclogite, epidote (Ep)–eclogite and phengite (Phn)–eclogite. They all occur as lenses within granitic and pelitic gneisses, or interlayers within marbles. Ky-eclogite occurs as a large (~800 m wide and 1700 m long; Fig. 2a) block. Ep-eclogite occurs as big

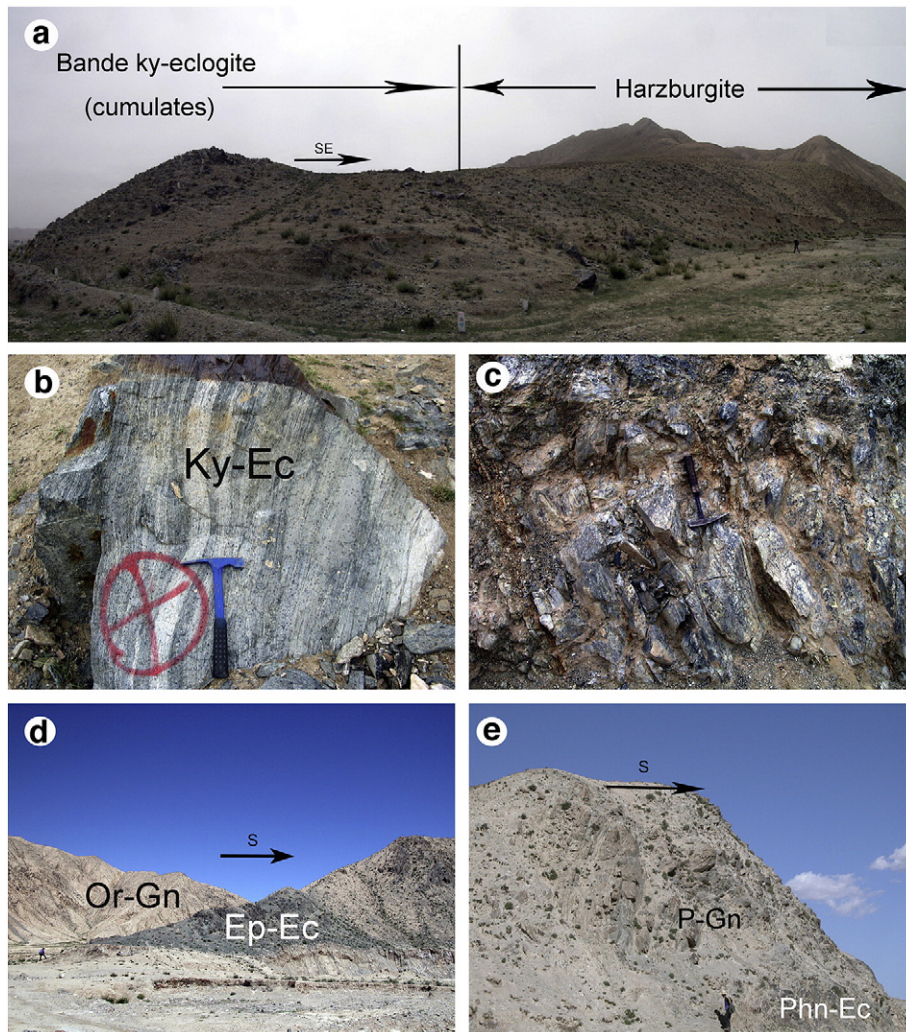


Fig. 2. Field views showing occurrence of serpentized harzburgite and three types of eclogite in Shaliuhe terrane, North Qaidam, China. (a) The field relationship between banded Ky-eclogite and serpentized harzburgite. (b) Banded Ky-eclogite. (c) Serpentized harzburgite. (d) Ep-eclogite blocks in the paragneiss. (e) Phn-eclogite blocks in the pelitic gneiss.

Table 1  
Representative microprobe mineral analyses of harzburgite and eclogite from Shaliuhe terrane, North Qaidam UHP belt, China

	Harzburgite												Ky-eclogite			Ep-eclogite				Phn-eclogite			Phn-eclogite												
	4C14-1.11		4C12-1.22		4C20-2.11		4C30-7.1		4C30-1		4C14-2		4C12-2		4C30-7		4C30-8		4C30-9		4C30-11		2D07			4C33			5S102			4C46			
	OI <sup>1</sup>	OI <sup>1</sup>	OI <sup>1</sup>	OI <sup>1</sup>	OI <sup>1a</sup>	OI <sup>2</sup>	OI <sup>2</sup>	OI <sup>2a</sup>	Opx <sup>a</sup>	Opx <sup>a</sup>	Opx <sup>a</sup>	Cpx-L <sup>a</sup>	Grt	Omp	Phn	Grt	Omp	Ep <sup>1</sup>	Ep <sup>2</sup>	Grt	Omp	Phn	Grt	Omp	Phn	R-Grt	C-Grt	Omp	Phn						
SiO <sub>2</sub>	40.60	41.02	40.78	40.81	41.20	41.06	41.22	41.84	56.22	56.34	56.19	53.54	40.78	55.31	52.46	39.54	56.91	39.83	38.51	38.87	56.48	51.49	39.51	37.97	55.39	52.14									
TiO <sub>2</sub>	0.00	0.00	0.00	0.03	0.00	0.06	0.02	0.03	0.00	0.00	0.03	0.06	0.01	0.06	0.37	0.00	0.05	0.07	0.14	0.02	0.00	0.44	0.01	0.07	0.04	0.50									
Al <sub>2</sub> O <sub>3</sub>	0.00	0.00	0.00	0.11	0.02	0.00	0.01	0.00	3.36	3.25	3.34	2.43	23.16	8.05	27.37	22.81	11.63	32.93	28.62	22.37	9.83	26.43	21.60	21.06	8.68	28.96									
Cr <sub>2</sub> O <sub>3</sub>									0.65	0.50	0.61	0.74	0.00	0.05	0.18	0.00	0.00	0.00	0.03	0.03	0.23	0.00	0.00	0.00	0.03	0.12									
FeO	9.23	9.25	9.42	11.03	8.28	5.01	5.64	3.43	5.81	5.83	6.11	1.45	17.27	2.10	1.03	20.34	4.43	1.61	6.01	24.00	3.71	1.55	22.16	24.23	3.59	1.26									
MnO	0.16	0.19	0.16	0.21	0.14	0.67	0.26	1.43	0.20	0.18	0.18	0.14	0.36	0.00	0.01	0.42	0.08	0.08	0.02	0.34	0.04	0.01	0.73	3.21	0.04	0.00									
NiO	0.38	0.35	0.32	0.25	0.28	0.27	0.31	0.14	0.19	0.10	0.08	0.21																							
MgO	50.04	50.28	49.98	48.42	50.73	53.28	53.09	53.53	34.37	34.71	34.22	17.09	12.24	11.81	4.11	9.23	8.94	0.07	0.18	5.85	9.29	3.73	4.53	0.97	10.67	3.37									
CaO	0.00	0.00	0.00	0.00	0.00	0.03	0.00	0.02	0.24	0.18	0.25	24.07	7.37	17.25	0.00	8.29	11.803	24.103	23.105	9.39	15.15	0.00	12.20	12.43	16.30	0.01									
Na <sub>2</sub> O	0.12	0.01	0.01	0.03	0.00	0.00	0.01	0.01	0.00	0.00	0.03	0.42	0.00	4.87	0.50	0.02	5.80	0.00	0.03	0.03	5.97	0.33	0.08	0.05	5.43	0.45									
K <sub>2</sub> O	0.06	0.00	0.00	0.00	0.01	0.00	0.01	0.00	0.00	0.00	0.00	0.01	0.00	0.01	10.49	0.00	0.02	0.01	0.01	0.01	0.00	10.35	0.00	0.00	0.00	9.46									
Total	100.59	101.10	100.67	100.89	100.66	100.38	100.57	100.43	101.04	101.09	101.05	100.15	101.26	99.54	96.52	100.65	99.69	98.73	96.68	100.98	100.70	94.33	100.82	99.99	100.17	96.27									
Si	0.99	0.99	0.99	1.00	1.00	0.99	0.99	1.00	1.92	1.92	1.92	1.94	2.99	1.97	6.86	2.97	2.04	3.00	3.00	2.98	2.00	6.90	3.04	3.02	1.97	6.79									
Ti	0.00	0.00	0.00	0.00	0.00	0.00	0.00	0.00	0.00	0.00	0.00	0.00	0.00	0.00	0.04	0.00	0.00	0.00	0.01	0.00	0.00	0.04	0.00	0.00	0.00	0.05									
Al	0.00	0.00	0.00	0.00	0.00	0.00	0.00	0.00	0.13	0.13	0.13	0.10	2.00	0.34	4.22	2.02	0.49	2.92	2.63	2.02	0.41	4.17	1.96	1.97	0.36	4.45									
Cr									0.02	0.01	0.02	0.02	0.00	0.00	0.02	0.00	0.00	0.00	0.00	0.00	0.01	0.00	0.00	0.00	0.00	0.01									
Fe <sup>3+</sup>									0.01	0.01	0.01	0.01	0.00	0.00	0.00	0.04	0.00	0.10	0.39	0.00	0.00	0.00	0.00	0.00	0.01	0.00									
Fe <sup>2+</sup>	0.19	0.19	0.19	0.23	0.17	0.10	0.11	0.07	0.16	0.16	0.17	0.03	1.06	0.06	0.11	1.24	0.13			1.54	0.11	0.17	1.42	1.61	0.10	0.14									
Mn	0.00	0.00	0.00	0.00	0.00	0.01	0.01	0.03	0.01	0.01	0.01	0.00	0.02	0.00	0.00	0.03	0.00	0.01	0.00	0.02	0.00	0.00	0.05	0.22	0.00	0.00									
Ni	0.01	0.01	0.01	0.01	0.01	0.01	0.01	0.00	0.01	0.00	0.00	0.01																							
Mg	1.82	1.82	1.81	1.76	1.83	1.91	1.90	1.90	1.75	1.76	1.74	0.92	1.34	0.63	0.80	1.03	0.48	0.01	0.02	0.67	0.49	0.75	0.52	0.12	0.56	0.65									
Ca	0.00	0.00	0.00	0.00	0.00	0.00	0.00	0.00	0.01	0.01	0.01	0.93	0.58	0.66	0.00	0.67	0.45	1.95	1.93	0.77	0.57	0.00	1.01	1.06	0.62	0.00									
Na	0.01	0.00	0.00	0.00	0.00	0.00	0.00	0.00	0.00	0.00	0.00	0.03	0.00	0.34	0.13	0.00	0.40	0.00	0.00	0.00	0.41	0.09	0.01	0.01	0.37	0.11									
K	0.00	0.00	0.00	0.00	0.00	0.00	0.00	0.00	0.00	0.00	0.00	0.00	0.00	0.00	1.75	0.00	0.00	0.00	0.00	0.00	0.00	1.77	0.00	0.00	0.00	1.57									
Total	3.01	3.01	3.01	3.00	3.00	3.01	3.01	3.00	4.00	4.00	4.00	4.00	8.00	4.00	13.92	8.00	4.00	7.99	7.98	8.01	4.00	13.90	8.00	8.00	4.00	13.77									
Mg <sup>#</sup>	90.6	90.7	90.4	88.7	91.6	95.0	94.4	96.5	91.6	91.8	91.2	96.5																							

Garnet: Fe<sup>2+</sup>/Fe<sup>3+</sup> ratios estimated by charge-balance method on a stoichiometric sum of cations, Omphacite: Fe<sup>3+</sup>=Na-(Al+Cr).

<sup>a</sup> From Zhang et al., 2005a, Cpx-L: Cpx exsolution lamellae in Opx, R-Grt: rim of garnet, C-Grt: core of garnet, Mg<sup>#</sup>=100Mg/(Mg+Fe).

(~100–200 m) lenses within granitic gneisses south of a fault (Fig. 2d). Phn-eclogite forms small lenses (~50–80 cm) within pelitic gneisses (Fig. 2e), or interlayers and lenses within marbles located towards the south of the cross section. As shown in Fig. 1c, the harzburgite occurs as blocks with varying size in ortho- and para-gneisses. The largest is a lensoid block (~500 m wide and 1400 m long) within the banded kyanite–eclogite (Fig. 1c and d). The harzburgite blocks are in gradational contact with eclogites (Fig. 2a). The harzburgite is strongly serpentinized with black and dark green colors (Fig. 2c). Gneisses are the principal lithology covering about 80% of the North Qaidam UHP belt, and both granitic and pelitic gneisses occur in Shaliuhe area.

### 3. Petrography and mineral chemistry

Minerals (Table 1) of representative harzburgite and eclogite samples were analyzed using a JEOL JXA-8100 electron probe at Peking University. The data are given in Table 1. The analytical conditions are: (1) accelerating voltage, 15 keV, (2) beam current, 10 nA, (3) 30 s counting at peak and 10 s on background. The instruments were calibrated for each element analyzed using well characterized natural and synthetic mineral as standards. The precisions were better than  $\pm 2\%$  for most elements.

#### 3.1. Serpentinized harzburgite

It mainly consists of serpentine, olivine, relict orthopyroxene and minor chromites. Olivine is replaced by serpentine

in mesh texture while orthopyroxene is replaced by talc. Magnetite and tremolite as by-products of serpentinization are ubiquitous.

Estimated primary modal abundance for olivine is ~75%, but most of them have been serpentinized. Two generations of olivine can be distinguished based on composition and inner texture. The first generation ( $Ol^1$ ) occurs as relic of serpentinized olivine, varying in size from 0.1 to 1 mm (Fig. 3a). Some larger  $Ol^1$  relics show kink bands (Fig. 3b). In NiO (wt.%) vs. Fo [100 Mg/(Mg+Fe)] diagram,  $Ol^1$  displays similar compositions to present-day abyssal peridotites (Fig. 4a) with Fo values 88.7–91.6 and NiO contents 0.28–0.44 wt.% (Table 1). In contrast, the second generation ( $Ol^2$ ) has much higher Fo (94–97) and contains a great number of small fluid inclusions (Fig. 3c, Table 1). Olivine with so high Fo content is obviously of metamorphic origin resulting from recrystallization of pre-cursive serpentine (Bruce et al., 2000).

Orthopyroxene (Opx) is typically replaced by talc and serpentine with only relics (0.5–5 mm) preserved in some samples (Fig. 3a). It varies in compositions (En 88.3–91.1;  $Al_2O_3$ , 2.69–4.63 wt.%; CaO, 0.15–1.62 wt.%;  $TiO_2$  <0.6 wt.%) (Table 1), and has higher  $Al_2O_3$  and CaO compared to Opx from the garnet peridotite exposed in the Luliangshan area of the UHP belt (Song et al., 2007). In  $Al_2O_3$  (wt.%) vs. Mg# [100 Mg/(Mg+Fe)] diagram, the entire data plot in the present-day abyssal peridotite field and differ distinctively from Opx in garnet peridotites of Sulu and North Qaidam (Fig. 4b). Clinopyroxene (Cpx) exsolution lamellae are well preserved in orthopyroxene (Fig. 3d),

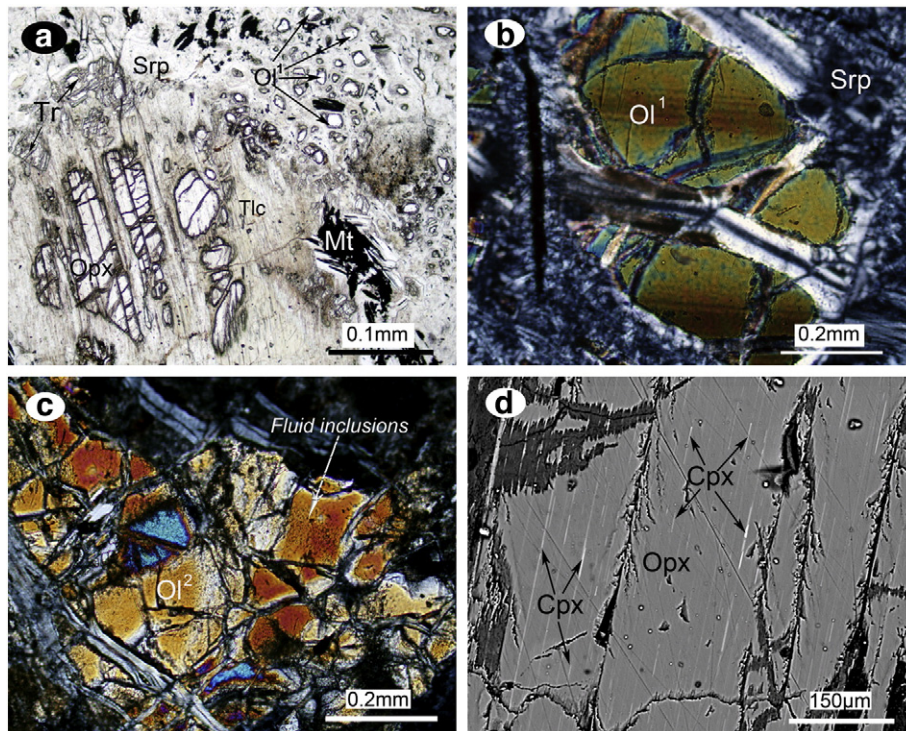


Fig. 3. Photomicrographs of harzburgite, Shaliuhe, North Qaidam, China. (a) The first generation of relic olivine ( $Ol^1$ ) and relict orthopyroxene (Opx), talc as coronas surround relict opx; Mt: Magnetite, Tr: tremolite (plane polarized light). (b) Kink bands of  $Ol^1$  (cross polarized light). (c) The second generation of relic olivine ( $Ol^2$ ), a lot of small fluid inclusions inside can be observed (plane polarized light). (d) Orthopyroxene, showing oriented clinopyroxene (Cpx) exsolution (back-scattered image).

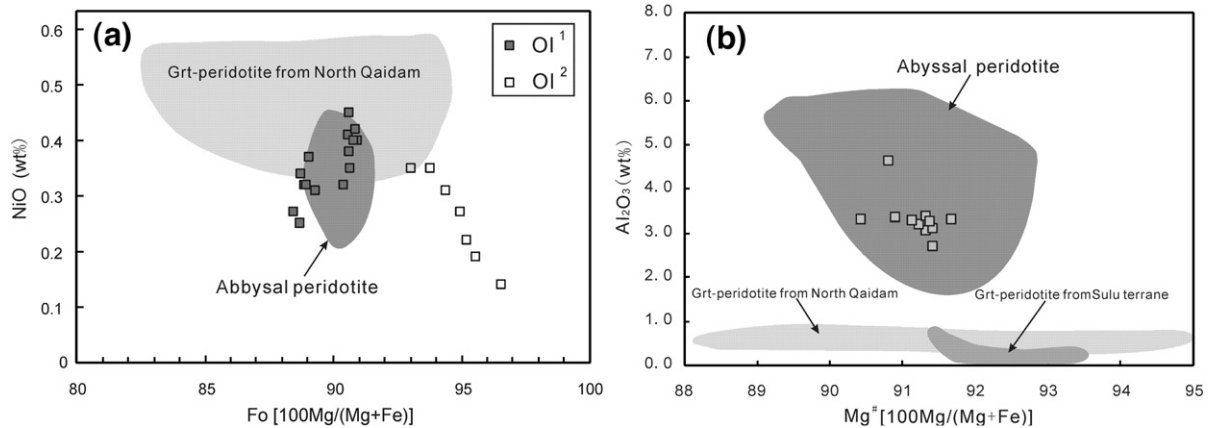


Fig. 4. (a)  $Mg^{\#}$  vs. wt.% NiO in olivine in harzburgite. (b) Cation ratio  $100 Mg/(Mg+Fe_{total})$  vs. wt.%  $Al_2O_3$  in orthopyroxene in harzburgite (modified from Zhang et al., 2005a). The field of abyssal peridotite is taken from Dick (1989), Niu and Hékinian (1997a,b); field of garnet peridotites in the North Qaidam is from Song et al. (2007) and in the Sulu UHP terrane is from Zhang et al. (2000) and Yang and Jahn (2000).

even in Opx pseudomorphs because clinopyroxene is more resistant against alteration (Aumento and Loubat, 1971).

Almost all serpentine occurs as very fine grain aggregation with mesh texture, around both relict olivine one ( $Ol^1$ ) and olivine two ( $Ol^2$ ) (Fig. 3b and, c). Because the metamorphic olivine ( $Ol^2$ ) with so high Fo content as mentioned above maybe result from the recrystallization of the precursor serpentine, there should be not less than two generations of serpentine minerals in these serpentinized harzburgites, i.e., the earliest serpentine originated from the first generation of olivine ( $Ol^1$ ) and the latest serpentine from the second metamorphic olivine ( $Ol^2$ ). Nevertheless, it is hard to identify them under microscope correctly.

### 3.2. Eclogites

#### 3.2.1. Kyanite–eclogite

Most of the well-preserved samples are coarse-grained with banded structure (Fig. 2b) defined by modal variation of pink garnet-rich and green omphacite-rich layers. The eclogite also has kyanite, rutile and varying amounts of coexisted phengite and quartz. The freshest samples contain 40–55% modal garnet, 40–45% omphacite, 10–15% kyanite, <2% rutile and minor phengite. The garnet-rich layers have much more abundant of kyanite than that of omphacite-rich layers. Garnet is usually coarse porphyroblast with large grain size (about 5 mm on average, and >10 mm for largest grain), surrounded by kyanite and omphacite (Fig. 5a). In addition, garnet porphyroblasts contain abundant mineral inclusions, which vary in type and abundance from grain to grain. Garnet grains from the garnet-rich layers contain abundant kyanite, epidote/zoisite, anorthite and minor chlorite and quartz. Garnet grains from the omphacite-rich layers contain lesser kyanite, plagioclase, epidote/zoisite and amphibole. Garnet is characterized with high MgO- and low FeO-contents, showing irregular compositional variations (almandine 31–38 mol%, pyrope 40–55 mol%, and grossular 17–24 mol%) (Table 1; Fig. 6a). Omphacite is partially replaced by cryptocrystalline symplectites of cpx+pl, which changed into amphi-

bole+pl in intensely amphibolitized samples. The jadeite content of matrix omphacite ranges from 25 to 30 mol% (Fig. 6b). Quartz lamellae, which were examined by EMP, are widespread in the centre of omphacite. These quartz lamellae are about 2–4  $\mu m$  wide and 50–200  $\mu m$  long, paralleling to the long axis of omphacite (Fig. 5b). Coesite pseudomorphs have been identified in omphacite (Fig. 5c). Kyanite is a common peak-stage mineral due to high Al-content protolith, rimmed by corona of plagioclase. Phengite with  $\sim 3.45$  Si-content is a minor phase (less than 1%).

#### 3.2.2. Epidote–eclogite

Well-preserved eclogites are composed of garnet, omphacite with varying amount of epidote, rutile and quartz (Fig. 5d), and display medium to coarse-grained texture. Garnet compositions vary in a range of almandine 33–42 mol%, pyrope 34–42 mol%, and grossular 21–27 mol% (Fig. 6a). Omphacite has 33–44 mol% jadeite (Fig. 6b). Most omphacite grains show rutile exsolutions (Fig. 5e), probably due to the change of temperature (Zhang et al., 2003; Malaspina et al., 2006). Epidote occurs as a common peak stage phase coexisting with garnet and omphacite. Epidote of the pre-peak metamorphic stage has higher  $Fe^{3+}/(Fe^{3+}+Al)$  ( $Ep^2$ : about 0.13) than that of the peak stage ( $Ep^1$ : 0.03–0.05) (Table 1). The retrograde stage epidote and zoisite are coarse grained porphyroblasts that replace earlier minerals.

#### 3.2.3. Phengite–eclogite

The peak assemblage of well-preserved Phn-eclogites is garnet+omphacite+phengite+rutile (Fig. 5f), and show fine-grained, granular texture. Most of them consist of 40–45% modal content of garnet, 40–50% omphacite, 10–15% phengite and about 5% rutile. Compared to garnet in Ky-eclogite and Ep-eclogite, garnet in Phn-eclogites has higher FeO- and lower MgO-components; and varies in compositions (higher almandine 50–68 mol%, lower pyrope 13–24 mol% and grossular 20–34 mol%) (Fig. 6a). Some garnet grains show compositional zoning. Increasing MgO and decreasing MnO from core to rim (Table 1) suggest a steadily prograde metamorphic growth.

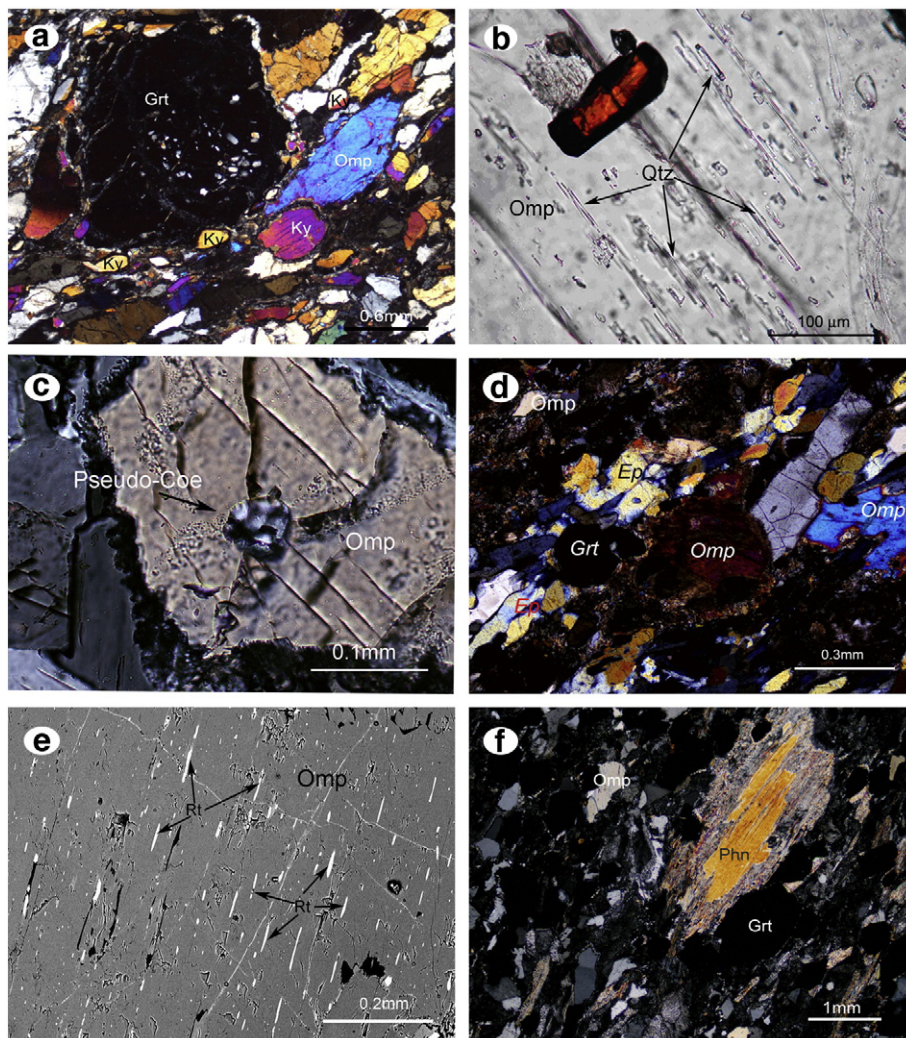


Fig. 5. Photomicrographs of three types of eclogite: Ky-eclogite (a, b and c), Ep-eclogite (d and e), Phn-eclogite (f) from Shaliuhe terrane, North Qaidam, China. (a) Xenoblastic garnet associated with omphacite and kyanite in Ky-eclogite (5S113, cross polarized light). (b) Exsolution quartz needles within omphacite in Ky-eclogite (2D07, plane polarized light). (c) Pseudomorphs of quartz after coesite in omphacite in Ky-eclogite (4C13, plane polarized light). (d) Omphacite has been partly replaced by cpx + pl coronas in Ep-eclogite (4C33, cross polarized light). (e) Rutile exsolution within omphacite in Ep-eclogite (2D43, BSE image). (f) Phengite associated with garnet and omphacite in Phn-eclogite (5S102, cross polarized light).

Omphacite has 33–45 mol% jadeite (Fig. 6b). Phengite has Si variation from 3.40 to 3.45 p.f.u. (Table 1).

### 3.3. Gneiss

Pelitic gneisses mainly consist of garnet-bearing muscovite–biotite schist with mineral assemblage of garnet–muscovite–biotite–plagioclase–k-feldspar–quartz and garnet-free muscovite–biotite schist with muscovite–biotite–plagioclase–k-feldspar–quartz. The granitic gneisses show coarse-grained granoblastic texture with strong foliation. They consist of k-feldspar, plagioclase, quartz, muscovite, and minor tourmaline. Because the strong regional amphibolite facies retrograde metamorphism, there is no relict HP index mineral assemblages existed in both gneisses. However, the petrological characteristics and mineral assemblage of garnet-bearing pelitic gneisses are quite similar to those gneisses in Northern Dulan, 20 km northwestward from the study area, in which coesite inclusions in

zircon have been reported by Yang et al. (2001) and Song et al. (2003a).

## 4. *P–T* determination

### 4.1. Eclogite

The Grt–Omp–Phn (–Ky) geothermobarometer of Ravna and Terry (2004) was used to calculate peak metamorphic conditions of the eclogite. Common end members were calculated in garnets using  $Fe^{2+}/Fe^{3+}$  ratios estimated by charge-balance method on a stoichiometric sum of cations. For omphacite,  $Fe^{3+}=Na-Al-Cr$  is used. Highest  $Mg/(Mg+Fe^{2+})$  content compositions at, or close to, garnet grain rims have been used to determine the peak *P–T* conditions (Carswell et al., 1997), as listed in Table 1. Most omphacite and phengite display extensive down pressure retrograde replacement reactions. Their compositions may have been modified. We thus selected

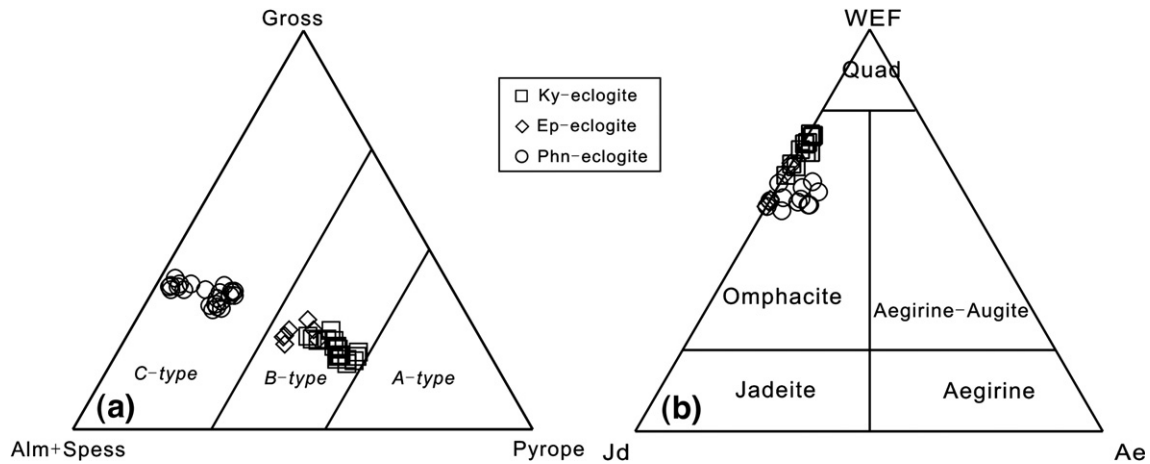


Fig. 6. Ternary diagrams showing compositional difference in garnet and omphacite for three types of eclogite from Shaliuhe terrane, North Qaidam, China. (a) Garnet plotted after Coleman et al. (1965), (*A-type*: pyrope > 55 mol% in garnet, *B-type*: pyrope 30–55 mol%, *C-type*: pyrope < 30 mol%), Gross symbol for grossular, Alm for almandine, Spess for spessartine. (b) Omphacite plotted after Morimoto (1988), WEF symbols for wollastonite + enstatite + ferrosilite, Jd for jadeite, Ae for aegirine.

the omphacite with highest jadeite content (Holland, 1980) and phengite with highest Si content (Massonne and Schreyer, 1987). Using the coexisting peak stage assemblage of Grt + Omp + Ky + Phn + Qtz for kyanite–eclogite, intersections of the Grt–Cpx, Grt–Cpx–Ky–SiO<sub>2</sub> and the Grt–Cpx–Phn curves yield  $P=2.7\text{--}3.4\text{ GPa}$ ,  $T=610\text{--}700\text{ }^{\circ}\text{C}$  (Fig. 7a and b). Using the Grt–Cpx–Phn peak stage assemblage for phengite–eclogite, intersection of the Grt–Cpx thermometer and Grt–Phn–Cpx barometer curves give  $P=2.7\text{ GPa}$ ,  $T=645\text{ }^{\circ}\text{C}$  (Fig. 7c).

#### 4.2. Serpentinized harzburgite

$P$ – $T$  conditions of harzburgite are estimated by single-pyroxene barometry (Mercier, 1980) and  $T_{\text{Al-Cr}}$  thermometry using different compositions (Witt-Eickschen and Seck, 1991). The  $T_{\text{Al-Cr}}$  thermometry is used to estimate the temperature, considering the effect of Cpx exsolution. The Cpx exsolution results in transformation of calcium in orthopyroxene, but no

obvious aluminum change. The average temperature ( $1012 \pm 37\text{ }^{\circ}\text{C}$ ) we obtained is consistent with the equilibrium temperature of mantle condition. Precise indicators, unfortunately, are not available to better constrain the pressure (Mével, 2003). Nevertheless, aluminum content in Opx has a negative correlation with pressure. Using single-pyroxene barometry (Mercier, 1980), the calculated metamorphic pressures for this meta-harzburgite are about  $1.3 \pm 0.2\text{ GPa}$  which should be the lowest stable pressure of serpentinized harzburgite. This is because the upper limited pressure of antigorite is hard to determine.

### 5. Geochemistry

#### 5.1. Analytical methods

Thirty less-retrogressed eclogite samples (Table 2) (8 Ky-eclogite, 7 Ep-eclogite and 15 Phn-eclogite) are analyzed for bulk-rock compositions.

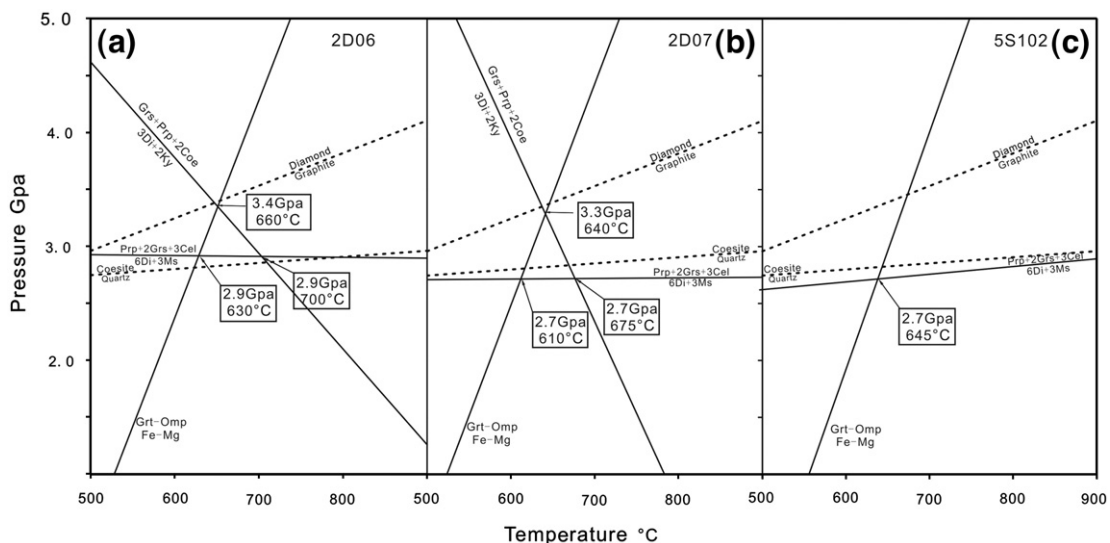


Fig. 7.  $P$ – $T$  diagrams for samples with assemblage Grt + Omp + Phn + Ky for Ky-eclogite (a and b) and one Phn-eclogite sample with assemblage Grt + Omp + Phn (c) (see error brackets in Ravna and Terry 2004).

Table 2  
Representative of Major and trace element analyses of Shaliuhe eclogites, North Qaidam UHP belt, China

Rock type	Ky-eclogite									Ep-eclogite						Phn-eclogite													
Analysis	2D04	2D05	2D06-1	2D07	2D08-1	4C05	4C08	5S113	2D32	2D41	2D43	4C18	4C33	4C34	4C36	4C41	4C42	4C46	4C48	5S81	5S101	5S102	5S103	2D51	2D52	2D53	2D54	2D55	2D56
<i>Major element oxide (wt.%)</i>																													
SiO <sub>2</sub>	50.15	48.84	47.27	47.39	48.53	49.09	48.69	48.29	49.26	47.25	47.42	47.95	47.13	48.20	46.38	46.25	49.51	48.88	49.84	48.34	50.09	48.02	49.10	48.00	44.95	47.75	52.11	49.28	47.04
TiO <sub>2</sub>	0.31	0.23	0.19	0.33	0.34	0.20	0.18	0.24	0.54	1.45	1.77	0.45	1.25	1.38	1.47	2.43	1.52	1.21	1.59	0.82	1.32	1.70	1.62	2.28	2.39	2.66	2.00	2.51	2.31
Al <sub>2</sub> O <sub>3</sub>	17.19	17.49	17.34	20.60	19.70	22.69	19.60	19.14	16.83	15.61	14.88	16.00	16.18	15.79	15.85	13.63	14.04	14.04	13.67	16.03	14.76	14.28	14.04	16.50	17.43	16.12	17.07	17.43	16.62
Fe <sub>2</sub> O <sub>3</sub> T	6.01	5.50	6.13	5.49	5.04	3.77	5.07	5.45	8.11	11.62	11.58	6.35	10.25	11.10	11.20	20.33	14.99	13.03	14.89	10.95	13.36	16.44	15.05	15.03	17.11	14.99	12.81	13.45	13.95
MnO	0.11	0.10	0.13	0.09	0.10	0.07	0.09	0.13	0.14	0.18	0.20	0.13	0.16	0.18	0.18	0.26	0.21	0.19	0.21	0.20	0.22	0.24	0.22	0.20	0.23	0.20	0.18	0.19	0.22
MgO	9.92	11.19	13.48	9.47	10.80	7.16	9.90	10.04	9.27	8.00	9.00	9.91	7.74	7.75	7.76	5.24	6.39	7.24	6.40	8.01	7.00	6.40	6.43	3.78	4.38	4.17	1.89	2.39	4.52
CaO	13.26	13.07	10.85	12.72	12.45	13.68	12.69	13.35	13.48	12.32	12.41	12.53	13.06	11.40	12.57	9.45	10.03	10.61	9.96	11.74	9.40	9.66	10.31	8.98	9.98	9.32	7.69	9.32	9.58
Na <sub>2</sub> O	2.43	2.15	1.97	2.02	2.00	2.54	2.25	2.05	2.26	2.47	2.23	1.96	2.36	2.62	2.14	1.85	2.14	2.19	2.15	1.52	2.03	2.24	2.32	2.86	2.43	3.14	3.31	3.23	2.96
K <sub>2</sub> O	0.14	0.17	0.06	0.15	0.09	0.31	0.27	0.12	0.09	0.13	0.05	0.66	0.13	0.19	0.17	0.14	0.36	0.34	0.14	0.43	0.29	0.11	0.14	0.73	0.38	0.54	1.07	1.01	1.02
P <sub>2</sub> O <sub>5</sub>	0.01	0.01	0.01	0.02	0.02	0.01	0.01	0.02	0.01	0.01	0.01	0.01	0.01	0.01	0.01	0.42	0.13	0.09	0.17	0.08	0.13	0.13	0.11	0.32	0.38	0.32	0.51	0.52	0.24
LOI	0.93	1.48	1.31	0.75	1.00	1.38	1.27	0.66	0.75	0.97	0.89	2.74	0.89	0.59	0.83	0.43	0.98	0.88	0.62	1.22	0.76	0.69	0.50	1.77	0.26	0.88	1.29	1.09	1.63
Total	100.46	100.22	98.74	99.03	100.07	100.90	100.02	99.49	100.75	100.03	100.44	98.69	99.16	99.21	98.56	100.42	100.31	98.71	99.63	99.34	99.36	99.92	99.84	100.46	99.92	100.10	99.92	100.42	100.09
<i>Trace elements (ppm)</i>																													
Cr	501	790	678	466	564	533	422	585	207	117	172	363	152	81	174	6.2	132	160	160	343	196	120	136	30.1	35.8	39.2	12.3	19.4	50.9
Ni	169	254	212	188	173	150	205	184	105	54.4	44.3	165	53.6	48.3	55.7	9.3	48.6	65.7	58.1	125	84.6	61.5	62.5	17.2	16.7	16.2	6.8	8.8	23.6
Rb	7.83	12.91	12.15	10.49	14.65	20.9	20.4	8.03	4.58	3.48	1.63	39.6	6.09	9.87	4.89	4.40	13.32	10.76	3.06	19.2	11.35	3.39	3.3	26.2	11.14	14.0	35.6	30.6	35.9
Ba	23.4	28.8	38.0	33.1	38.1	41.6	30.1	30.7	24.7	72.8	12.0	101	61.1	48.3	105	24.6	92.8	132	31.1	110	157	65.1	57.5	274	105	246	343	221	347
Th	0.03	0.03	0.10	0.21	0.18	0.03	0.37	0.07	0.01	0.01	0.01	0.03	0.00	0.02	0.15	1.72	0.67	0.50	0.78	0.35	0.76	0.75	0.98	2.50	2.13	2.73	7.77	5.13	2.19
U	0.02	0.03	0.06	0.03	0.08	0.02	0.03	0.03	0.02	0.03	0.02	0.05	0.06	0.04	0.08	0.40	0.25	0.23	0.35	0.13	0.29	0.31	0.30	0.62	0.61	0.77	1.74	1.30	0.51
Nb	0.18	0.21	0.21	0.22	0.26	0.21	0.14	0.27	0.15	0.14	0.02	0.34	0.02	0.12	0.06	8.18	4.86	3.95	6.08	2.41	4.55	5.49	5.19	18.67	14.24	23.50	39.05	40.60	19.46
Ta	0.02	0.02	0.02	0.02	0.03	0.01	0.01	0.03	0.02	0.02	0.01	0.03	0.01	0.01	0.01	0.64	0.36	0.29	0.40	0.19	0.36	0.42	0.39	1.32	1.06	1.65	2.98	2.87	1.39
La	0.57	0.63	0.50	1.82	1.57	0.60	2.28	0.80	0.71	0.61	0.28	0.68	0.64	0.68	1.61	13.98	5.53	4.37	4.49	3.07	5.79	5.17	6.04	15.98	13.78	19.76	43.25	30.66	14.80
Ce	1.53	1.96	1.07	3.97	3.50	1.45	3.76	2.10	2.10	2.68	1.24	1.99	2.69	2.46	3.78	36.97	14.56	11.26	13.10	7.97	15.35	13.59	15.69	34.71	30.46	42.41	91.12	64.71	31.69
Pr	0.27	0.24	0.17	0.53	0.49	0.22	0.41	0.35	0.41	0.66	0.36	0.37	0.67	0.54	0.75	5.63	2.21	1.70	2.20	1.23	2.32	2.07	2.58	4.42	4.11	5.43	11.35	8.46	4.15
Sr	175	197	145	208	243	351	227	210	250	230	301	520	354	224	271	160	85	232	110	166	126	76.6	83.5	236	141	216	183	221	351
Nd	1.66	1.28	1.23	2.73	2.21	1.29	1.78	2.05	2.73	4.77	3.08	2.38	5.04	3.85	5.41	29.59	11.62	9.07	10.59	6.71	12.63	11.04	12.94	20.60	18.68	25.16	48.73	37.49	18.23
Zr	8.17	9.03	9.89	11.11	12.15	6.09	4.63	7.63	7.36	9.67	5.39	11.53	8.84	9.55	10.36	185.99	88.55	74.76	96.30	41.58	78.17	91.70	95.55	108.43	114.45	116.70	323.34	247.99	113.76
Hf	0.33	0.31	0.20	0.35	0.30	0.22	0.17	0.28	0.35	0.62	0.48	0.44	0.62	0.62	0.79	5.01	2.36	1.99	2.53	1.24	2.22	2.61	2.67	2.85	3.07	3.06	8.84	6.56	3.00
Sm	0.67	0.48	0.46	0.87	0.79	0.46	0.49	0.71	1.10	1.98	1.58	0.97	2.13	1.58	2.24	8.20	3.57	2.84	3.48	2.12	3.82	3.53	3.86	5.19	4.75	6.18	12.08	10.06	4.54
Eu	0.39	0.31	0.29	0.48	0.46	0.36	0.36	0.41	0.58	0.90	0.85	0.47	1.05	0.81	1.05	2.34	1.21	1.04	1.22	0.81	1.29	1.23	1.29	1.87	1.73	2.08	3.34	3.12	1.67
Gd	0.89	0.65	0.73	1.06	1.10	0.59	0.62	0.89	1.41	2.51	2.24	1.34	2.72	2.12	2.89	8.84	4.19	3.50	4.29	2.69	4.42	4.53	4.30	5.83	5.14	6.74	12.55	10.90	4.80
Tb	0.17	0.13	0.11	0.19	0.21	0.11	0.11	0.17	0.26	0.47	0.44	0.26	0.51	0.41	0.54	1.51	0.75	0.64	0.86	0.50	0.78	0.85	0.84	1.02	0.99	1.16	2.29	2.00	0.89
Dy	1.16	0.86	0.85	1.29	1.37	0.73	0.71	1.07	1.77	3.11	2.85	1.75	3.13	2.68	3.46	9.63	4.88	4.13	5.54	3.25	4.84	5.35	5.33	6.27	6.18	7.14	13.91	11.91	5.55
Y	6.94	4.92	6.01	7.44	9.17	4.16	4.19	6.46	10.27	18.17	16.35	10.62	17.47	15.94	19.96	58.41	30.54	25.48	32.45	19.96	28.43	32.23	29.87	37.13	34.90	40.90	76.58	64.34	31.50
Ho	0.22	0.19	0.18	0.26	0.28	0.16	0.15	0.23	0.32	0.68	0.59	0.32	0.66	0.58	0.75	2.40	1.16	0.95	1.20	0.73	1.15	1.28	1.17	1.47	1.36	1.68	3.03	2.52	1.22
Er	0.62	0.42	0.51	0.71	0.84	0.37	0.35	0.60	0.95	1.70	1.48	0.98	1.61	1.49	1.83	5.69	2.87	2.40	3.50	1.94	2.80	3.10	3.30	3.60	3.71	4.04	8.39	6.90	3.36
Tm	0.09	0.05	0.07	0.11	0.14	0.04	0.04	0.08	0.13	0.26	0.22	0.14	0.24	0.22	0.27	0.91	0.45	0.38	0.53	0.31	0.46	0.51	0.51	0.58	0.56	0.64	1.25	1.02	0.51
Yb	0.62	0.44	0.48	0.75	0.84	0.38	0.37	0.64	0.92	1.68	1.43	1.01	1.57	1.46	1.76	5.90	3.00	2.52	3.28	2.07	3.08	3.42	3.14	3.83	3.47	4.16	7.74	6.36	3.15
Lu	0.09	0.06	0.07	0.11	0.12	0.05	0.05	0.09	0.13	0.24	0.20	0.15	0.23	0.22	0.26	0.90	0.46	0.39	0.49	0.31	0.47	0.53	0.46	0.58	0.51	0.63	1.13	0.93	0.47
[Gd/Yb]N	1.18	1.23	1.26	1.17	1.08																								

Whole-rock major elements were analyzed using a RIX-2100 X-ray fluorescence (XRF) spectrometer on fused glass disks at Peking University. All results are normalized against Chinese rock reference standard GBW07105, and analytical uncertainties range from  $\pm 1\%$  to  $\pm 5\%$ .

Whole-rock trace elements were analyzed using an Elan 6100-DRC inductively coupled plasma mass spectrometry (ICP-MS) after acid digestion of sample powders in Teflon bombs at Northwest University, Xi'an. Detailed analytical procedure is similar to that reported by Liu et al. (2001) and Song et al. (2007). Two USGS rock reference materials BCR-2 and BHVO-2 were used to monitor the analytical accuracy and precision. Analytical accuracy is ca.  $\pm 5\%$  for trace elements with abundances  $\geq 20$  ppm, and ca.  $\pm 10\%$  for elements  $\leq 20$  ppm.

Whole-rock Sr–Nd isotopic compositions of 14 fresh samples (Table 3; 2 Ky-eclogite, 3 Ep-eclogite and 9 Phn-eclogite) were analyzed in the Institute of Geology and Geophysics of Chinese Academy of Sciences, Beijing. The analytical procedure follows that by Jahn et al. (1996). The analyses were performed using a seven-collector Finnigan MAT262 mass spectrometer after the sample powders were digested/dissolved using HClO<sub>4</sub> and HF in Teflon vessels. Average procedural blanks are Sr=200 pg, Nd=60 pg. <sup>87</sup>Sr/<sup>86</sup>Sr ratios were normalized against <sup>86</sup>Sr/<sup>88</sup>Sr=0.1194 and all <sup>87</sup>Sr/<sup>86</sup>Sr ratios have been adjusted to NBS-987 Sr standard=0.710250. <sup>143</sup>Nd/<sup>144</sup>Nd ratios were normalized against <sup>146</sup>Nd/<sup>144</sup>Nd=0.7219, and have been adjusted to La Jolla Nd standard=0.511860 (Jahn et al., 1996). The uncertainty is  $\pm 1$ –2% for Rb,  $\pm 0.1\%$  for Sr, and  $\pm 0.2$ –0.5% for Sm and Nd depending on their concentration. The  $\epsilon_{Nd}(T)$  values are calculated based on the metamorphic ages following the method by Jahn (1999).

## 5.2. Major elements

The analytical data are given in Table 2. For all the three types of eclogite rocks, SiO<sub>2</sub> contents vary from about 45 to 52%. Kyanite–eclogite is characterized by lower TiO<sub>2</sub> (0.18–

0.34 wt.%), higher Al<sub>2</sub>O<sub>3</sub> (17.19–22.69 wt.%), MgO (7.16–13.48 wt.%) and CaO (10.85–13.68 wt.%) as expected from the modal mineralogy. Phengite–eclogite, on the other hand, has higher TiO<sub>2</sub> (1–2.43 wt.%) and FeO (9.85–18.3 wt.%), lower Al<sub>2</sub>O<sub>3</sub> (13.63–16.03 wt.%), MgO (1.89–8.11 wt.%) and CaO (7.69–11.74 wt.%). The epidote–eclogite displays a narrow range of compositions relative to Ky-eclogite and Phn-eclogite. The MgO varies from 7.75 to 9.91 wt.%, and Al<sub>2</sub>O<sub>3</sub>, from 14.88 to 16.83 wt.%.

Fig. 8 shows the variation trends of elemental abundances as a function of MgO. For major elements, FeO, TiO<sub>2</sub> and Na<sub>2</sub>O decrease and Al<sub>2</sub>O<sub>3</sub> and CaO increase with increasing MgO in all eclogites samples. This is consistent with mineralogical control of basaltic/gabbroic protoliths. For example, kyanite–eclogite is consistent with a troctolitic protolith, whereas the epidote–eclogite may have protoliths of plagioclase rich gabbros. On the other hand, phengite–eclogites are consistent with their protoliths being incompatible element enriched basaltic melts from primitive compositions (MgO~8 wt.%) to the more evolved ones with MgO<2 wt.% (Niu et al., 2002; Niu, 2005).

## 5.3. Trace elements

Incompatible elements such as Nb, Zr, U and REE (represented by Nd) are negatively correlated with MgO content (Fig. 8), whereas compatible elements such as Cr and Ni show positive correlations with MgO content. These are consistent with the above interpretations.

Ky-eclogites contain very low abundances of REE (average  $\Sigma$ REE=10.1 ppm, the lowest  $\approx 3 \times$  Chondrite) (Table 2). Four of the seven samples show similar LREE depletion ( $La_N/Sm_N=0.55$ –0.85). Other three samples (2D07, 2D08-1 and 4C08) display LREE enrichment ( $La_N/Sm_N=1.28$ –2.98). Moreover, all they show distinct positive Eu anomaly ( $Eu/Eu^*=1.51$ –2.08) (Table 2, Fig. 9a). Such characteristics is again consistent with their protolith being troctolitic with trapped interstitial liquid, which explains the low REE

Table 3  
Rb–Sr and Sm–Nd isotope compositions of three types of eclogites from Shaliuhe terrane, North Qaidam UHP belt, China

Sample no.	Rock type	[Rb] (ppm)	[Sr] (ppm)	<sup>87</sup> Rb/ <sup>86</sup> Sr	<sup>87</sup> Sr/ <sup>86</sup> Sr	$\pm 2\sigma$	$I_{Sr}$ (445 Ma)	[Sm] (ppm)	[Nd] (ppm)	<sup>147</sup> Sm/ <sup>144</sup> Nd	<sup>143</sup> Nd/ <sup>144</sup> Nd	$\pm 2\sigma$	$\epsilon_{Nd}(0)$	$\epsilon_{Nd}(T)$ $T=445$ Ma	$f(Sm/Nd)$
4C05	Ky-eclogite	20.4	355.5	0.16	0.704529	12	0.70349	0.46	1.26	0.2199	0.513052	19	8.1	6.8	0.12
4C08	Ky-eclogite	18.3	215.7	0.25	0.704612	11	0.70306	0.49	1.68	0.1753	0.512897	9	5.1	6.3	–0.11
2D32	Ep-eclogite	4.2	259.2	0.05	0.703508	14	0.70321	1.07	2.61	0.2489	0.513090	13	8.8	5.9	0.27
4C33	Ep-eclogite	5.7	369.5	0.04	0.703844	13	0.70356	1.97	4.57	0.2602	0.513160	10	10.2	6.6	0.32
4C36	Ep-eclogite	4.7	293.1	0.05	0.704288	11	0.70399	2.15	5.01	0.2598	0.513234	11	11.6	8.0	0.32
4C41	Phn-eclogite	4.2	158.2	0.08	0.705764	14	0.70528	7.66	26.56	0.1745	0.512772	14	2.6	3.9	–0.11
4C42	Phn-eclogite	11.1	82.0	0.39	0.710070	11	0.70762	3.83	12.37	0.1872	0.512793	15	3.0	3.6	–0.05
4C46	Phn-eclogite	9.6	212.9	0.13	0.708243	10	0.70742	2.67	8.42	0.1922	0.512837	11	3.9	4.1	–0.02
4C48	Phn-eclogite	5.6	108.4	0.15	0.709010	12	0.70806	3.57	11.25	0.1917	0.512814	12	3.4	3.7	–0.03
5S101	Phn-eclogite	10.3	125.4	0.24	0.708981	11	0.70747	3.77	12.22	0.1866	0.512820	11	3.6	4.1	–0.05
5S102	Phn-eclogite	3.2	75.2	0.12	0.708601	26	0.70780	3.08	9.40	0.1983	0.512838	12	3.9	3.8	0.01
2D51	Phn-eclogite	24.8	240.2	0.30	0.711513	12	0.70962	4.93	19.06	0.1565	0.512590	13	–0.9	1.4	–0.20
2D53	Phn-eclogite	12.9	215.0	0.17	0.715700	12	0.71460	5.90	23.32	0.1529	0.512612	11	–0.5	2.0	–0.22
2D55	Phn-eclogite	28.6	216.8	0.38	0.712875	9	0.71046	9.36	34.31	0.1649	0.512616	8	–0.4	1.4	–0.16

Decay constants used: <sup>87</sup>Rb=0.0142 Ga<sup>–1</sup> (Steiger and Jager, 1977), <sup>147</sup>Sm=0.00654 Ga<sup>–1</sup> (Lugmair and Marti, 1978).

$\epsilon_{Nd} = [(^{143}Nd/^{144}Nd)_{sample} / (^{143}Nd/^{144}Nd)_{CHUR} - 1] \times 10000$ ,  $f_{Sm/Nd} = [(^{147}Sm/^{144}Sm)_{sample} / (^{147}Sm/^{144}Nd)_{CHUR}] - 1$ ,  $(^{143}Nd/^{144}Nd)_{CHUR} = 0.512638$ ,  $(^{147}Sm/^{144}Nd)_{CHUR} = 0.1967$ .

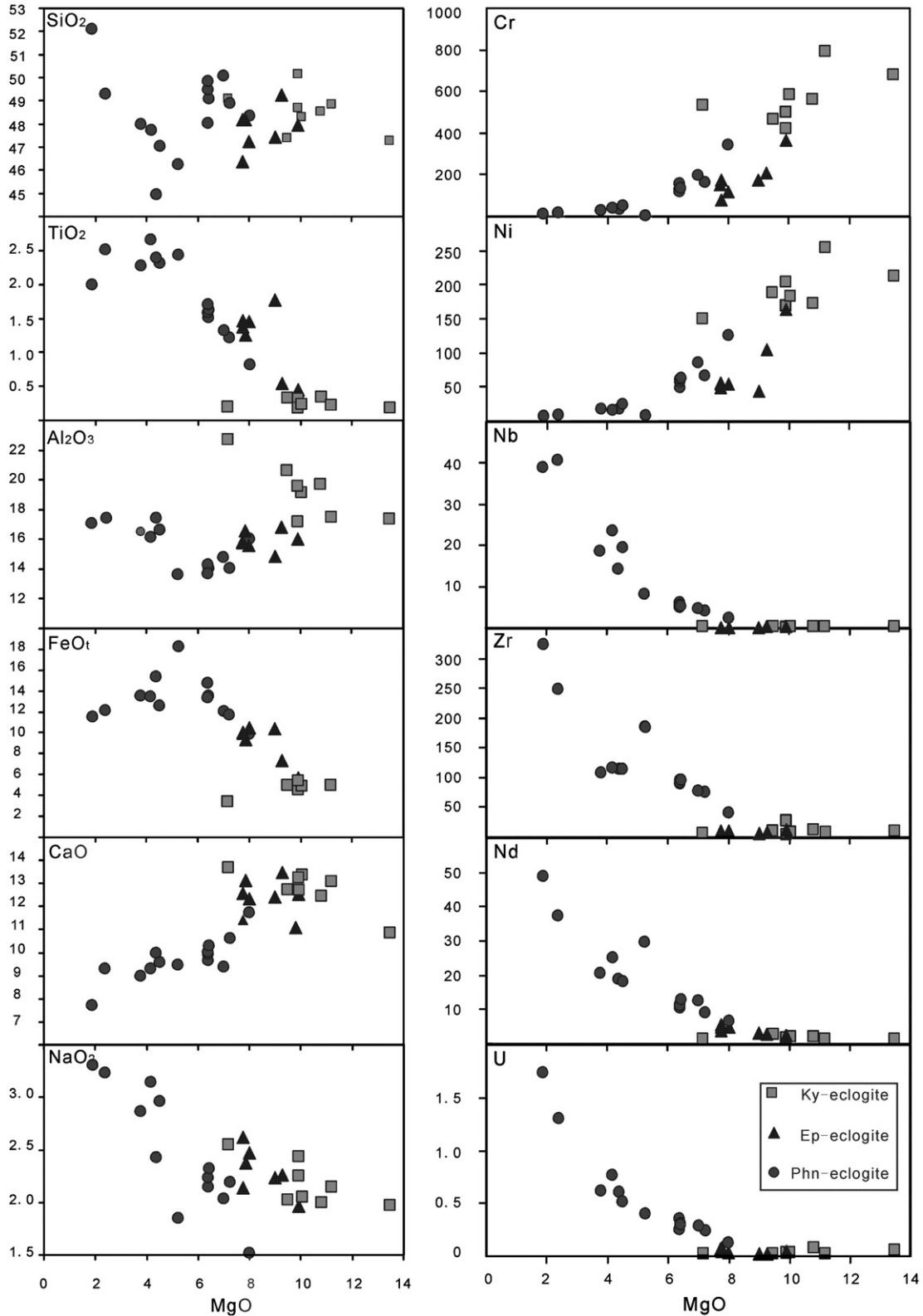


Fig. 8. Whole-rock major and trace elements variations as a function of MgO for eclogites from Shaliuhe terrane, North Qaidam UHP belt, China.

abundances, positive Eu anomalies, and varying degrees of LREE enrichment (Niu et al., 2002). The REE enrichment could also be enhanced by a melt percolation, refertilization, or “metasomatism” as widely invoked (Jahn et al., 2003a).

The Ep-eclogites display REE patterns characterized with LREE depletion ( $La_N/Sm_N=0.12-0.46$ ), and show distinct positive Eu anomaly ( $Eu/Eu^*=1.24-1.42$ ) (Table 2, Fig. 9c). These are again consistent with plagioclase rich gabbroic

protoliths, which also explains the conspicuous positive Eu anomalies in most samples of this group. Such protoliths can very well explain other trace elements as well. For example, positive Sr anomalies, as is Eu anomalies, are expected with plagioclase rich protoliths.

In primitive-mantle-normalized spidergrams (Fig. 9b and d), Ky- and Ep-eclogites show similar characteristics with strong enrichment of Sr and depletion of Th, Nb and Zr. Depletion of high field strength elements such as Nb, Ta, Zr, Hf, Th and to a lesser extent Ti are incompatible elements that prefer to stain in the melt, thus depleted in the cumulate troctolitic and gabbroic

rocks. Metasomatic refertilization enriched not only REEs, but also other large ion lithophile elements like Rb, Ba, U etc. (e.g., Niu et al., 2002).

Phn-eclogite samples from blocks in gneisses display flat REE patterns without Eu anomaly ( $Eu/Eu^* = 0.84–1.04$ ) (Fig. 9e). Meanwhile, Phn-eclogite samples associated with marbles show strong LREE enrichment ( $La_N/Yb_N = 2.85–4.01$ ), and their LREE abundance varies from  $45.33$  to  $129.40 \times$  chondrite and HREE from  $21.24$  to  $53.49 \times$  chondrite (Fig. 9g). Enriched basalts are likely the best candidate protoliths for these Phn-eclogite samples. The varying degree of crystallization can

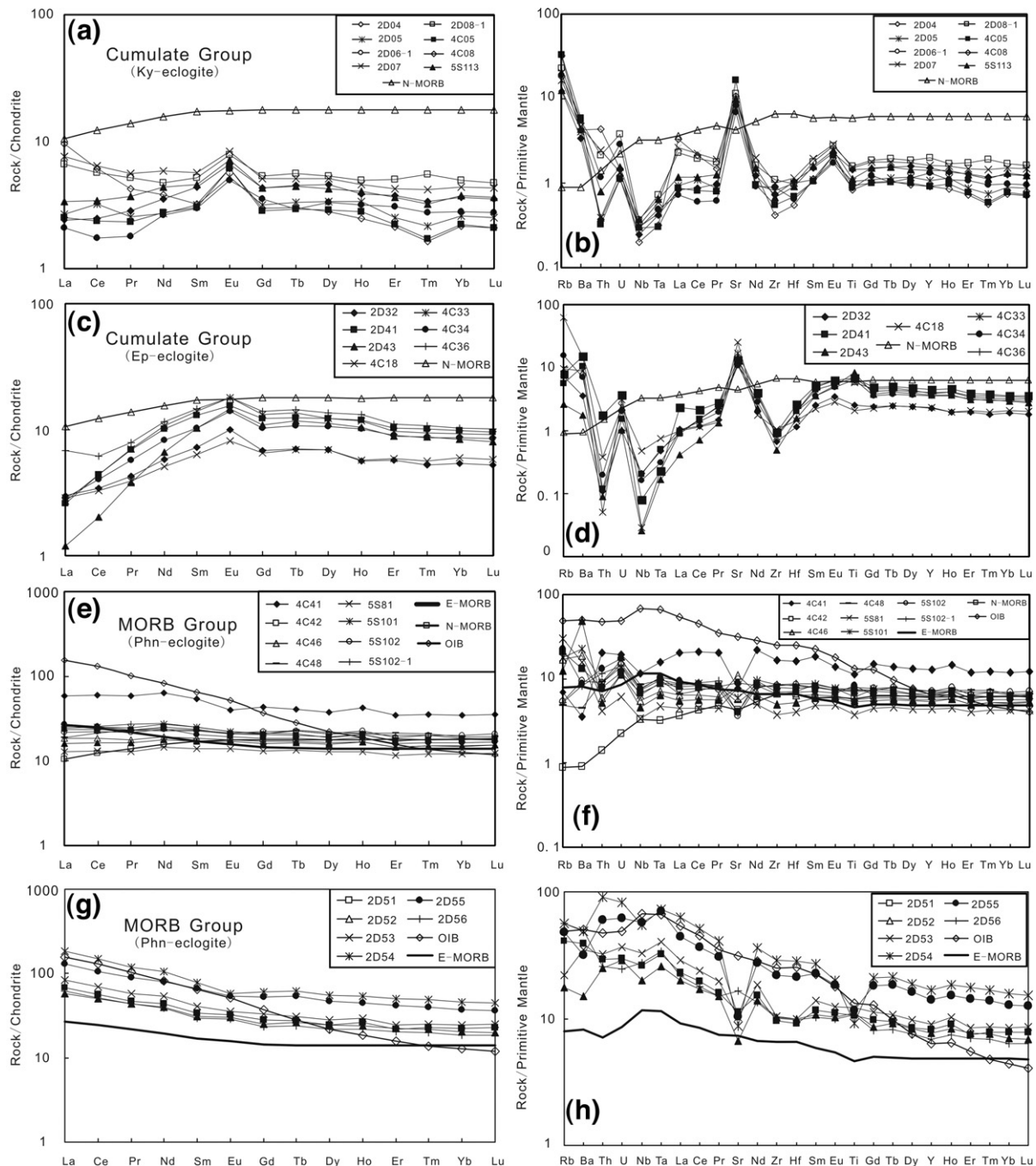


Fig. 9. Chondrite-normalized REE patterns and Primitive Mantle-normalized spidergrams of three types eclogites from the Shaliuhe terrane, North Qaidam, China. (a and b) Cumulate group of protoliths of Ky-eclogites. (c and d) Cumulate group of Ep-eclogites. (e–h) MORB group of Phn-eclogites.

(i.e., the LLDs) not only explains major and trace systematics on MgO variation diagrams (Fig. 8), but also relative abundance levels of REE and other elements in Fig. 9. Negative anomalies of Sr, Eu and Ti are consistent with high degrees of crystallization (removal) of plagioclase and titanomagnetite (low MgO melt).

#### 5.4. Whole-rock Rb–Sr and Sm–Nd isotopes

The Ky-eclogite and Ep-eclogite samples of troctolitic/gabbroic protoliths have restricted range of present-day  $^{87}\text{Sr}/^{86}\text{Sr}$  ratios (0.703–0.705). Phn-eclogite samples, on the other hand, have a wide range of present-day  $^{87}\text{Sr}/^{86}\text{Sr}$  ratios (0.705–0.716).

For Sm–Nd isotopes, Ky-eclogite and Ep-eclogite samples have  $^{147}\text{Sm}/^{144}\text{Nd}$  higher than the chondritic value of about 0.1967 (except for sample 4C08), and restricted  $^{143}\text{Nd}/^{144}\text{Nd}$  ratios (0.512–0.513). Phn-eclogite samples have relatively high

$^{143}\text{Nd}/^{144}\text{Nd}$  ratios restricted in a range from 0.5125 to 0.5128), but  $^{147}\text{Sm}/^{144}\text{Nd}$  values lower than the chondritic value. For the measured Nd isotope ratios,  $\epsilon_{\text{Nd}}(0)$ , three Phn-eclogite samples have slightly negative value (–0.4 to –0.9), and the rest of Phn-eclogite samples have relatively lower value than Ky-eclogite and Ep-eclogite.

The relationship between  $\epsilon_{\text{Nd}}(T)$  ( $T=445$  Ma) and  $^{147}\text{Sm}/^{144}\text{Nd}$  is shown in Fig. 10a. All eclogites from Shaliuhe terrane show positive  $\epsilon_{\text{Nd}}(T)$  values, suggesting their protoliths being of oceanic crust origin, similar to eclogites in Alpine and Hercynian orogenic belts (Tilton et al., 1991; Von Quadt et al., 1997), but different from those of the Dabie and Sulu terrane with clearly continental origin (Liou et al., 1996, 1997; Jahn, 1999; Jahn et al., 2003a,b).

Both Ky- and Ep-eclogite samples show essentially the same Sr–Nd isotopic compositions with  $I_{\text{Sr}}(445 \text{ Ma})=0.703$ –0.704 and  $\epsilon_{\text{Nd}}(445 \text{ Ma})=5.9$ –8.0. On the other hand, Phn-

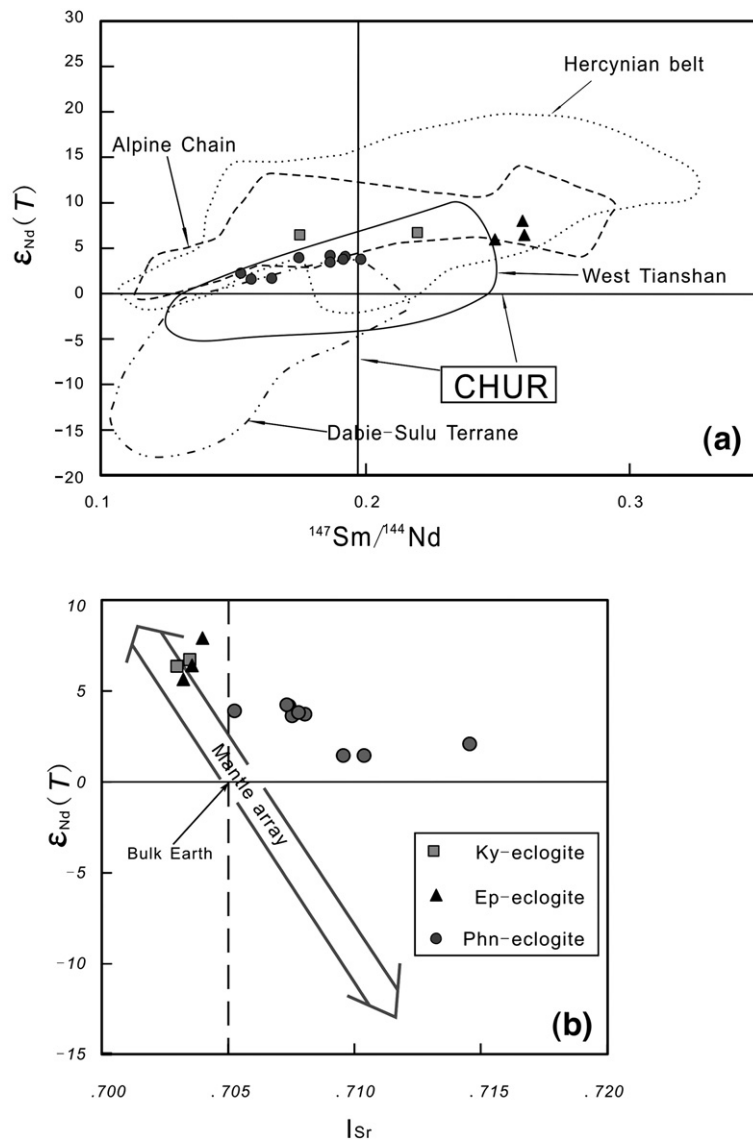


Fig. 10. (a)  $\epsilon_{\text{Nd}}(T)$  vs.  $^{147}\text{Sm}/^{144}\text{Nd}$  plots for eclogite from Shaliuhe terrane ( $T=445$  Ma). Data sources for Alpine Chain, Hercynian Belt and Dabie–Sulu Terrane are from Appendix of Jahn (1999); West Tianshan is from Zhang et al. (2005c, 2007); (b)  $\epsilon_{\text{Nd}}(T)$  vs.  $I_{\text{Sr}}$  plots for eclogites from Shaliuhe terrane.  $\epsilon_{\text{Nd}}(T)$  and  $I_{\text{Sr}}$  are calculated at 445 Ma.

eclogite samples display significant Sr–Nd isotopic compositions ( $I_{Sr}$  (445 Ma)=0.705–0.715 and  $\epsilon_{Nd}$  (445 Ma)=1.4–4.1) (Fig. 10b), with the “trend” deviating from the mantle array. Their  $\epsilon_{Nd}$  (445 Ma)>0 is consistent with “straightforward” mantle origin of the protolith, whereas their  $I_{Sr}$  (445 Ma) = ~0.706 to 0.716 is not. Except for sample 2D53 with high  $I_{Sr}$  (445 Ma)=0.716, all other samples of this group exhibit significant positive Rb/Sr– $I_{Sr}$  trend (not shown), and negative  $\epsilon_{Nd}$ – $I_{Sr}$ , suggesting that these rocks may have experienced a hydrous melt (high Rb/Sr vs. moderately high Nd/Sm) metasomatism in the history of these rocks, probably in the early stage of subduction.

## 6. U–Pb zircon dating

### 6.1. Analytical techniques

After the selected sample 5S23 (Kyanite–eclogite) was crushed and sieved, zircons were separated by magnetic and heavy liquid techniques before finally handpicking under a binocular microscope. The separated zircon grains and zircon standard Temora (417 Ma, Black et al., 2003) were embedded in 25 mm epoxy discs and then polished down to approximately half thickness. The internal structure was examined using cathodoluminescence (CL) images on a FEI PHILIPS XL30 SFEG SEM with 2-min scanning time at conditions of 15 kV and 120  $\mu$ A, at Peking University. Mineral inclusions in zircons were identified using laser Raman micro-spectroscopy at Peking University. U, Th and Pb were analyzed by SHRIMP II at Beijing SHRIMP center, Chinese Academy of Geosciences.

Instrumental conditions and measurement procedures were similar to those reported earlier (Compston et al., 1992; Stern, 1998; Williams, 1998). CL images and optical photomicrographs were taken as a guide for locating U–Pb dating spots. Spot sizes were typically 25–30  $\mu$ m, using a 9 nA primary  $O_2^-$  ion beam. Age determination for each spot was collected in sets of 5 scans through the mass stations with count times of 2 to 20 s. The Temora zircon standard used for U–Pb calibration, was analyzed after every 3–4 analyses of our samples. The squid (Ludwig, 2002) and isoplot (Ludwig, 1997) programs were used for data processing and measured  $^{204}Pb$  was applied for the common lead correction. Results are given in Table 4 with  $2\sigma$  errors.

### 6.2. Zircon internal structure and SHRIMP data

Most zircon crystals from kyanite–eclogite are subhedral and rounded with 100 to 250  $\mu$ m in diameter (Fig. 11). Ten of the 21 zircon grains selected for analysis have core–rim distinctions in CL images (Fig. 11a and b). The cores show obvious dark oscillatory zoning, whereas the rims are characterized by irregular, cloudy-zoned or fir-tree zoning CL patterns with stronger luminescence than the cores, similar to zircons from granulite-facies rocks (Vavra et al., 1996) and eclogite or gabbro (Rubatto et al., 1999; Rubatto and Gebauer, 2000). Other zircon grains show homogeneous CL pattern without relict oscillatory zoning core (Fig. 11c). A few eclogite-facies inclusions of garnet, omphacite and rutile are identified in zircons without zoning and in rim portions of zircons with zoning (Fig. 11d). Most analyses (Table 4) show low to medium

Table 4  
U, Th and Pb SHRIMP zircon data of kyanite–eclogite from Shaliuhe terrane, North Qaidam UHP belt, China

Sample	Domain	$^{206}Pb_c$ [%]	U [ppm]	Th [ppm]	Th/U	$^{206}Pb^*$ [ppm]	$^{207}Pb^*/^{206}Pb^*$	$\pm\%$	$^{207}Pb^*/^{235}U$	$\pm\%$	$^{206}Pb^*/^{238}U$	$\pm\%$	$^{206}Pb/^{238}U$ Age	
5S23-1.1	Rim	10.01	32.02	0.98	0.03	2.13	0.0380	85.0	0.360	85.0	0.0697	5.8	434	$\pm 25$
5S23-2.1	Core	1.13	343.71	346.24	1.04	24.30	0.0574	5.3	0.642	5.8	0.0812	2.2	503	$\pm 11$
5S23-3.1	Core	1.23	268.97	258.87	0.99	18.70	0.0525	6.8	0.578	7.2	0.0799	2.2	496	$\pm 10$
5S23-3.2	Rim	2.76	93.26	2.86	0.03	5.84	0.0552	12.0	0.539	12.0	0.0708	2.6	441	$\pm 11$
5S23-4.1 <sup>a</sup>	Core	0.80	180.44	174.81	1.00	12.10	0.0580	5.2	0.618	5.6	0.0773	2.3	480	$\pm 11$
5S23-5.1 <sup>a</sup>	Rim	6.10	57.88	1.58	0.03	3.54	0.0400	37.0	0.370	37.0	0.0668	3.3	417	$\pm 13$
5S23-6.1	Rim	3.51	101.60	1.51	0.02	6.28	0.0649	9.9	0.621	10.0	0.0694	3.5	433	$\pm 15$
5S23-7.1	Rim	2.88	99.61	1.31	0.01	6.24	0.0503	15.0	0.491	15.0	0.0708	2.6	441	$\pm 11$
5S23-8.1 <sup>a</sup>	Core	0.80	331.34	443.12	1.38	22.80	0.0567	4.4	0.620	4.9	0.0794	2.2	492	$\pm 10$
5S23-10.1	Core	0.60	406.39	538.76	1.37	29.50	0.0578	3.5	0.669	4.1	0.0840	2.1	520	$\pm 11$
5S23-11.1	Rim	3.03	99.22	1.30	0.01	6.16	0.0577	14.0	0.558	15.0	0.0701	2.6	437	$\pm 11$
5S23-12.1	Rim	2.40	98.68	1.42	0.01	6.14	0.0566	15.0	0.552	15.0	0.0707	2.7	440	$\pm 12$
5S23-13.1	Core	0.92	232.34	280.34	1.25	17.00	0.0599	5.3	0.699	5.9	0.0846	2.7	524	$\pm 14$
5S23-13.2	Rim	3.63	58.37	0.71	0.01	3.75	0.0500	24.0	0.500	24.0	0.0720	3.0	448	$\pm 13$
5S23-14.1	Core	1.07	201.85	191.66	0.98	14.70	0.0609	5.9	0.706	6.3	0.0841	2.2	520	$\pm 11$
5S23-14.2	Rim	2.26	127.49	2.99	0.02	8.25	0.0586	14.0	0.595	14.0	0.0736	2.5	458	$\pm 11$
5S23-15.1	Core	1.76	264.51	263.94	1.03	20.40	0.0534	7.8	0.647	8.1	0.0880	2.2	544	$\pm 11$
5S23-16.1	Rim	6.13	40.26	0.76	0.02	2.61	0.0540	28.0	0.530	28.0	0.0708	3.6	441	$\pm 15$
5S23-17.1 <sup>a</sup>	Core	0.54	266.01	300.79	1.17	17.80	0.0566	4.5	0.605	5.0	0.0774	2.2	481	$\pm 10$
5S23-17.2 <sup>a</sup>	Rim	3.46	49.02	0.69	0.01	3.04	0.0642	12.0	0.616	13.0	0.0696	3.0	434	$\pm 12$
5S23-18.2	Rim	2.36	58.78	0.87	0.02	3.68	0.0773	10.0	0.759	11.0	0.0712	2.8	444	$\pm 12$
5S23-19.1	Rim	2.80	115.41	2.60	0.02	7.67	0.0533	14.0	0.552	14.0	0.0752	2.5	467	$\pm 11$
5S23-20.1	Core	0.88	288.61	261.73	0.94	20.80	0.0578	4.8	0.662	5.3	0.0832	2.2	515	$\pm 11$
5S23-20.2	Rim	1.88	44.60	1.06	0.02	2.76	0.0836	6.9	0.814	7.5	0.0706	3.0	440	$\pm 13$
5S23-21.1	Rim	3.31	110.59	2.06	0.02	7.09	0.0615	14.0	0.612	14.0	0.0722	2.6	449	$\pm 11$

<sup>a</sup> Data are not used for age determination.

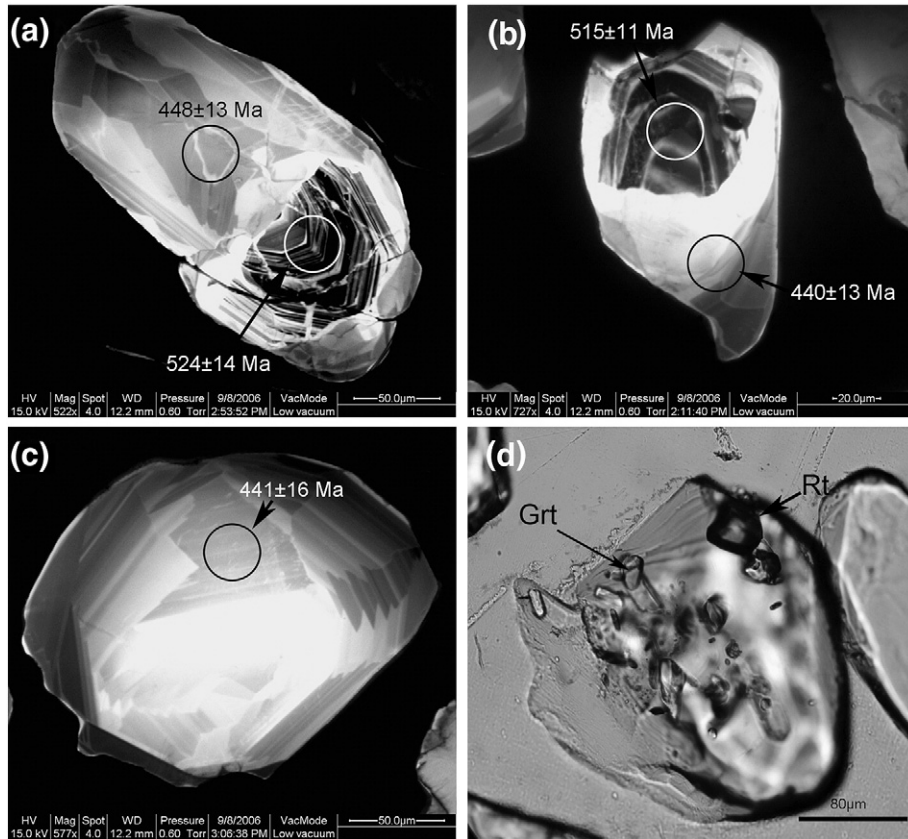


Fig. 11. Photomicrographs of zircons from the Ky-eclogite (sample 5S23) showing cathodoluminescence (CL) images, mineral inclusions and SHRIMP U–Pb ages. (a)–(b) showing core-rim structure zircon CL images, oscillatory zoning cores and fir-tree zoning rims. (c) No core-rim structure zircon showing similar fir-tree zoning CL pattern. (d) Garnet and rutile inclusions in zircon (plane-polarized light).

U contents (~41–406 ppm) with the oscillatory zoning cores having higher U content than the gray-luminescent rims. Thorium contents also show distinction between cores (very

high, 174.81–538.76 ppm) and rims (very low, 0.69–2.99 ppm). So Th/U ratios are variably high for cores (~0.939–1.392), but very low for rims (~0.013–0.031). This

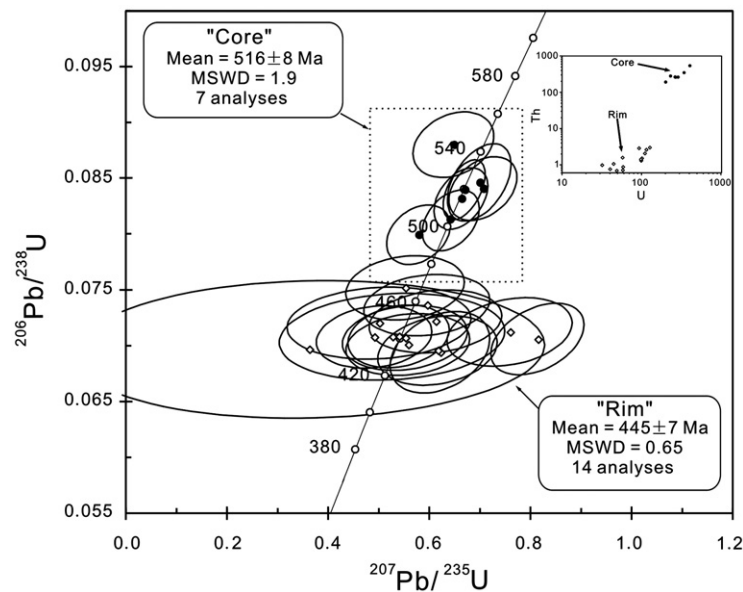


Fig. 12. Concordia diagram showing results of zircon SHRIMP analyses from the Ky-eclogite (sample 5S23). Data-point error ellipses are  $2\sigma$ . Square: data used for rim age determination; circle: data are used for core age determination. The inserted small figure shows the  $\log(\text{Th ppm})$  vs.  $\log(\text{U ppm})$ , including all core and rim age determination data.

difference is also well presented on Fig. 12. Ten analyses of zircon cores yielded  $^{204}\text{Pb}$ -corrected  $^{206}\text{Pb}/^{238}\text{U}$  ages ranging from  $480 \pm 11$  Ma to  $544 \pm 11$  Ma. Three small relict cores ( $<25\mu\text{m}$  in size) have mixed younger ages ( $480 \pm 11$  Ma,  $481 \pm 10$  Ma and  $492 \pm 10$  Ma). Therefore, we excluded them when obtaining a weighted average age. These analyses plot on Concordia (Fig. 12), and define a concordia age of  $516 \pm 8$  Ma ( $n=7$ ) for zircon cores. Fifteen analyses of zircon rims yielded younger  $^{206}\text{Pb}/^{238}\text{U}$  ages ( $\sim 417 \pm 13$  Ma to  $479 \pm 25$  Ma). We excluded the youngest age ( $417 \pm 13$  Ma) for weighted averaging because of possible retrogressive resetting. We thus obtained a weighted rim age of  $445 \pm 7$  Ma ( $n=14$ ).

## 7. Discussion

More than 20 ultra-high pressure metamorphic terranes so far have been recognized on Earth (Carswell and Compagnoni, 2003a; Liou et al., 2004). Only a few of them, such as Zermatt–Saas Zone of the Western Alps (Reinecke, 1991; Bucher et al., 2005) and West Tianshan of China (Zhang et al., 2002a,b, 2005c, 2007), are interpreted to have been formed by deeply subducted oceanic crustal sequences. Eclogites and ultramafic rocks in most UHPM belts, such as the Dabie–Sulu of China (Jahn, 1999) and Western Gneiss Region of Norway (Carswell et al., 2003b), are interpreted to be of continental crust affinities on the basis of petrology and geochemistry. *In situ* tectonic relationships of eclogites, ultramafic rocks and the country felsic gneisses from these UHPM belts point to subduction and exhumation of the continental lithologies as a whole (Liou and Zhang, 2002; Zheng et al., 2003).

The lithological assemblages and the presence of coesite-bearing paragneisses are consistent with the North Qaidam UHPM belt being a type continental subduction/exhumation zone (Song et al., 2006). However, petrologic and geochemical data show that the rock association of the Shaliuhe cross section represents remnants of typical oceanic crust (vs. continental) assemblage that have undergone subduction-zone metamorphism before exhumed with its felsic gneisses.

### 7.1. Determination of ophiolitic lithology

Serpentinized harzburgite and three types of eclogite co-exist with apparent gradational contact between them in the Shaliuhe cross section. The primary mineral assemblage of the serpentinized harzburgite, olivine + orthopyroxene + chromite, represents a spinel-facies mantle peridotite. The apparent absence of clinopyroxene is consistent with the peridotite being harzburgite residues of high extents of mantle melting. The first generation olivine ( $\text{Ol}^1$ ) and orthopyroxene in the harzburgite are similar in composition to the present-day abyssal peridotite (Fig. 4), whereas the second-generation olivine ( $\text{Ol}^2$ ) has much higher Fo content (95–97). In addition,  $\text{Ol}^2$  has much higher Mn contents (0.26–1.43 wt.%) than that of  $\text{Ol}^1$  (0.14–0.21 wt.%). This difference has been recorded in olivines from Alpine peridotite with subduction-zone metamorphism history (Scambelluri et al., 1991). High Fo metamorphic olivines have also been observed in other ophiolitic suites (e.g., Bruce et al., 2000). We

suspect that the harzburgite might have experienced serpentinization (forming Mg-rich serpentines separated from magnetite trails) probably at shallow crustal levels before subducted and recrystallized. The de-serpentinization during prograde metamorphism can readily produce Fo-rich olivine through a reaction of the form: antigorite + brucite = olivine + H<sub>2</sub>O as discussed by Scambelluri et al. (1995). The small fluid inclusions within secondary olivine might be captured during this recrystallization process.

It is not straightforward to evaluate the prograde metamorphic conditions the harzburgite may have experienced, the estimated  $P$ – $T$  values ( $T=1012 \pm 37$  °C and  $P=1.3 \pm 0.2$  GPa), which are deep crustal or shallow mantle conditions, may be lower limits. The upper limited metamorphic pressure, which the serpentinized harzburgite undergone, is unknown; this is because the antigorite has the wide  $P$ – $T$  range (Wunder and Schreyer, 1997). Because of no fault contact between serpentinized harzburgite and Ky-eclogite as mentioned above, we infer that the serpentinized harzburgite associated with troctolitic/gabbroic eclogites maybe undergone HP-UHP metamorphism. However, the lack of garnet suggests that it may have never reached pressures in excess of  $\sim 3.0$  GPa, which requires that garnet be a stable phase in the harzburgite.

Three distinguished types of eclogites differ in mineral assemblages, mineral compositions and protolith types as discussed above. This variability of mafic protoliths is similar to that reported for the subducted oceanic crust of New Caledonia (Spandler et al., 2004). All Ky-eclogite and Ep-eclogite rocks are metamorphosed mafic cumulate rocks, whereas protoliths of Phn-eclogite resemble enriched-type MORB as found at ocean ridges and near-ridge seamounts (Sun and McDonough, 1989; Niu and Batiza, 1997). In terms of bulk-rock major and trace elements, the Ky-eclogite is consistent with a troctolitic protolith, and the Ep-eclogite is consistent with a plagioclase rich gabbroic protolith. We suggest that the banded structure of kyanite–eclogite is largely inherited from the cumulate layering with some metamorphic/deformational modification. Despite the likely metamorphic overprints, the Phn-eclogite still possesses compositional characteristics of enriched-type MORB (Figs. 8 and 9) (Sun and McDonough, 1989; Niu and Batiza, 1997). The major and trace element variation as a function of MgO (Fig. 8) is readily explained by fractional crystallization from relatively primitive basalts (MgO  $\sim 8$  wt.%) to the more evolved ones.

The restricted Sr–Nd isotopic variation of the Ky-eclogite and Ep-eclogite with high  $\epsilon_{\text{Nd}}(T)$  and low  $I_{\text{Sr}}$  is also consistent with an ocean crust protolith derived from the depleted mantle (Fig. 12). The high  $\epsilon_{\text{Nd}}(T)$  is also consistent with the Phn-eclogite having an oceanic crustal protolith, including enriched-type MORB. The high and variable  $I_{\text{Sr}}$  (Fig. 10) is consistent with the fact that Sr is a mobile element (vs. Nd) and can be modified in the histories of these rocks including seafloor alteration and subduction-zone metasomatism. Crustal contamination would have affected both Sr and Nd isotopes, making the rocks remain along the mantle array towards low  $\epsilon_{\text{Nd}}(T)$  and high  $I_{\text{Sr}}$  end, but this is not the case.

Concerning the field relationship, Ep-eclogite, the largest lensoid block—Ky-eclogite and enclosed serpentinized

harzburgite may constitute the relict lower ophiolitic suite (Fig. 1d). Integrated with the Phn-eclogite, it is possible to establish an ophiolitic stratigraphy from mantle peridotite, to cumulate, and to upper basaltic rocks.

### 7.2. Tectonic evolution of the ophiolitic lithology

The peak metamorphic pressure is 2.7–3.4 GPa at 610–700 °C for Ky-eclogite and 2.7 GPa at 645 °C for Phn-eclogite calculated by the Grt-Omp-Phn(-Ky) geothermobarometer of Ravna and Terry (2004). In addition, abundant quartz needles and pseudomorphs of coesite in omphacite of Ky-eclogite also support the UHP metamorphism. All these observations suggest that the eclogites should have experienced UHP metamorphism. If the coexisting harzburgite had similar histories with the eclogite, then the lack of garnet in this harzburgite places a upper pressure limit, i.e., the peak pressure may have never reached ~3.0 GPa. It is possible that the harzburgite have different histories. That is, the eclogites are of UHPM origin, but the harzburgite may be not. However, the field relationships do not suggest so.

The shape and the CL patterns of zircons from kyanite-eclogite indicate that they record both magmatic and metamorphic events. We interpret the older magmatic core mean age of  $516 \pm 8$  Ma as representing the protolith age of kyanite-eclogite, and the younger rim mean age ( $445 \pm 7$  Ma) as representing the UHP metamorphic age. The latter age is similar to the whole-rock Sm–Nd and Zircon U–Pb ages of ~460 Ma in Dulan terrane (Song et al., 2003b, 2006), but younger than that of westward Yuka and Xitieshan terranes (Menold et al., 2002; Zhang et al., 2005b). This maybe due to the oblique subduction from west to east in Qaidam UHP belt. The previous U–Pb dating of metamorphic zircons from Altyn Tagh, Yuka and Xitieshan eclogites gave 750–800 older magmatic core ages of eclogite protolith (Yang et al., 2003; Zhang et al., 2005b; Liu et al., 2007). Because there is more than 250 Ma gap between the protolith and metamorphic ages, they suggested that the protoliths of eclogites in Altyn Tagh, Yuka and Xitieshan terranes in this UHP belt were formed in the Late Proterozoic rifting event and once resided in a continental setting, and then had been subducted to the mantle depth with continental materials during the Paleozoic (Yang et al., 2003; Zhang et al., 2005b; Liu et al., 2007). Our studies show that the protolith and metamorphic ages of eclogites in Shaliuhe section are  $516 \pm 8$  Ma and  $445 \pm 7$  Ma respectively, which suggests that the Paleo-Qilian ocean had existed before Cambrian and final closed in Early Ordovician, there is no large time gap for the residence of paleo-oceanic crust in continental setting. Song et al. (2006) obtained a 423 Ma age for the coesite-bearing paragneiss in the North belt of Dulan, which should represent the age of continental subduction. This time lag is similar to what was documented in Alps, where there may be ~10–15 Ma time delay between oceanic crust subduction (Zermatt-Saas ophiolite) and subduction of continental crust (Dora-Maira Massif) (Rubatto et al., 1998). Therefore, we conclude that the ophiolitic sequence in the Shaliuhe cross section had not been resided in the continent crust before subducting, but the relict of consumed oceanic lithosphere.

The oceanic subduction may be initiated along the oceanic-continent crust transition where abundant sediments were accumulated (Regenauer-Lieb et al., 2001). Flexural bending and stress concentration produced by sediment loading may have caused subduction initiation, and oceanic plate subduction. Therefore, some continental materials (i.e., protoliths or both para- and ortho-gneisses) could be carried with the descending plate to UHPM depth. Paragneisses, which contain coesite-bearing zircon from Qaidam UHP metamorphic belt, may be the product of these passive continental margin materials and then exhumed to Earth's surface. In addition, no convincing UHP evidence has been found for granitic gneisses, which constitute ~80 vol.% of this UHP metamorphic belt. There are several possibilities: (1) there have been few in-depth studies of the granitic gneiss so far; (2) there may be metastable preservation of these volumetrically significance rocks, as seen in other HP/UHP localities (Tilton et al., 1997; Krabbendam et al., 2000); (3) the granitic gneisses may have never been subducted. Therefore, there was probably no large-scale continental subduction, which is different from Dabie–Sulu UHP belt in eastern China.

UHPM eclogites of oceanic protolith (or ophiolitic assemblage) are rarely observed in continental-type UHP terrains (Coleman and Wang, 1995; Carswell and Compagnoni, 2003a). The main reason seems to be physical difficulties of exhumation. UHPM eclogites of oceanic protolith are rather dense. So far, several models have been proposed to explain the exhumation of HP metamorphic rocks of oceanic protoliths, such as accretionary wedge (Platt, 1986), diapiric model (Hall and Kincaid, 2001) and corner flow (Cloos, 1985). Recently, Hermann et al. (2000) proposed that the serpentinites, which are much less dense than the ambient mantle rocks, are the most likely carriers of dense eclogite. For Shaliuhe cross section in North Qaidam UHP belt, the metamorphic olivine ( $Ol^2$ ) related to the subduction zone metamorphism has been replaced by serpentine minerals strongly in studied samples (Fig. 3b and c). It is possible that the Shaliuhe UHPM eclogitic assemblage in North Qaidam UHP belt may indeed have resulted from diapiric rise of the highly serpentinitized harzburgites.

Compared with the classic continent-type UHP belt such as Dabie–Sulu in eastern China and Western Gneiss Region of Norway, there is a subducted oceanic crust preserved in North Qaidam UHP belt, Northwestern China. The study in this paper shows clearly that the evolution of North Qaidam UHP orogenic belt from oceanic subduction followed by continental subduction and collision, which is similar to the young Alpine and Himalayan orogenic belt (O'Brien, 2001). However, the relationship of the oceanic and continental subduction and subsequent collision in North Qaidam UHP belt needs to do the further study later on.

## 8. Conclusions

The Shaliuhe terrane is mainly made up of granitic and pelitic gneisses. Three types of eclogite and co-existing harzburgite exposed along the Shaliuhe cross section are studied in detail. Mineral data and metamorphic  $P$ – $T$  estimations indicate that the eclogites may have once been subducted to a depth of UHP conditions. The serpentinitized harzburgite is typical mantle

peridotite. It may have also been metamorphosed and subducted along the subduction zone, but the lack of garnet suggests that the peak pressure may be  $< \sim 3.0$  GPa. Geochemical and isotopic data suggest that the protoliths of these eclogites are of ocean crustal origin. The bulk lithological constitutes an ophiolitic stratigraphy. Zircon U–Pb SHRIMP dating shows that the protolith age is  $516 \pm 8$  Ma and the metamorphic age is  $445 \pm 7$  Ma. These data suggest that a Paleo-Qilian Ocean was developed between Qaidam and Qilian blocks before the early Ordovician. The Shaliuhe UHPM assemblages provide us with insights into the dynamic processes and histories of oceanic subduction, continental collision and exhumation.

## Acknowledgements

Our sincere thanks to G.M. Shu, Z.Y. Chu and X.M. Liu for their help with the laboratory work. Bin Chen is also appreciated for their constructive advisement, which helps make a better presentation of the final product. We are grateful to Drs. Hermann J. and Mattinson C.G. for their critical and constructive review on the manuscript. The National Natural Science Foundation of China (Grants 40325005 and 40773012), which is greatly appreciated financially supports this study.

## References

- Aumento, F., Loubat, H., 1971. The Mid-Atlantic Ridge near  $45^{\circ}$ N: serpentinized ultramafic intrusions. *Can. J. Earth Sci.* 8, 631–663.
- Black, L.P., Kamo, S.L., Allen, C.M., Aleinikoff, J.K., Davis, D.W., Korsch, R.J., Foudoulis, C., 2003. TEMORA 1: a new zircon standard for Phanerozoic U–Pb geochronology. *Chemical Geology* 200, 155–170.
- Bruce, M.C., Niu, Y., Harbort, T.A., Holcombe, R.J., 2000. Petrological, geochemical and geochronological evidence for a Neoproterozoic ocean basin recorded in the Marlborough terrane of the northern New England Fold Belt. *Australian Journal of Earth Sciences* 47, 1053–1064.
- Bucher, K., Fazis, Y., Capitani, C., Grapes, R., 2005. Blueschists, eclogites, and decompression assemblages of the Zermatt-Saas ophiolite: high-pressure metamorphism of subducted Tethys lithosphere. *American Mineralogist* 90, 821–835.
- Carswell, D.A., O'Brien, P.J., Wilson, R.N., Zhai, M.G., 1997. Thermobarometry of phengite-bearing eclogites in the Dabie Mountains of Central China. *Journal of Metamorphic Geology* 15, 239–252.
- Carswell, D.A., Compagnoni, R., 2003a. Introduction with review of the definition, distribution and geotectonic significance of ultrahigh pressure metamorphism. In: Carswell, D.A., Compagnoni, R. (Eds.), *EMU Notes in Mineralogy*, vol. 5. Eötvös University Press, pp. 3–9.
- Carswell, D.A., Cuthbert, S.J., 2003b. Ultrahigh pressure metamorphism in the Western Gneiss Region of Norway. In: Carswell, D.A., Compagnoni, R. (Eds.), *EMU Notes in Mineralogy*, vol. 5. Eötvös University Press, pp. 51–73.
- Cloos, M., 1985. Thermal evolution of convergent plate margins: thermal modeling and reevaluation of isotopic Ar-ages for blueschists in the Franciscan Complex, California. *Tectonics* 4, 421–433.
- Compston, W., Williams, I.S., Kirschvink, J.L., Zhang, Z., 1992. Zircon U–Pb ages for the Early Cambrian time-scale. *Journal of the Geological Society of London* 149, 171–184.
- Coleman, R.G., Wang, X.M., 1995. Overview of the geology and tectonics of UHPM. In: Coleman, R.G., Wang, X.M. (Eds.), *Ultrahigh Pressure Metamorphism*. Cambridge University Press, pp. 1–32.
- Coleman, R.G., Lee, L.D., Beatty, L.B., Brannock, W.W., 1965. Eclogites and eclogites: their differences and similarities. *Geological Society of America Bulletin* 76, 483–508.
- Dick, H.J.B., 1989. Abyssal peridotites, very slow spreading ridges and ocean ridge magmatism. In: Saunders, A.D., Norry, M.J. (Eds.), *Magmatism in the Ocean Basins*. Geological Society, London, Special Publications 42, 71–105.
- Ernst, W.G., 1988. Tectonic history of subduction zones inferred from retrograde blueschist  $P$ – $T$  paths. *Geology* 16, 1081–1084.
- Ernst, W.G., 2001. Subduction, ultrahigh-pressure metamorphism, and regurgitation of buoyant crustal slices implications for arcs and continental growth. *Physics of the Earth and Planetary Interiors* 127, 253–275.
- Hall, P.S., Kincaid, C., 2001. Diapiric flow at subduction zones: a recipe for rapid transport. *Science* 292, 2472–2475.
- Hermann, J., Müntener, O., Scambelluri, M., 2000. The importance of serpentinite mylonites for subduction and exhumation of oceanic crust. *Tectonophysics* 327, 225–238.
- Holland, T.J.B., 1980. The reaction albite=jadeite+quartz determined experimentally in the range 600–1200 °C. *American Mineralogist* 65, 125–134.
- Jahn, B.M., 1999. Sm–Nd isotope tracer study of UHP metamorphic rocks: implications for continental subduction and collisional tectonics. *International Geology Review* 41, 859–885.
- Jahn, B.M., Cornichet, J., Cong, B.L., Yui, T.F., 1996. Ultrahigh  $\epsilon_{\text{Nd}}$  eclogites from an ultrahigh pressure metamorphic terrane of China. *Chemical Geology* 127, 61–79.
- Jahn, B.M., Fan, Q.C., Yang, J.J., Henin, O., 2003a. Petrogenesis of the Maowu pyroxenite-eclogite body from the UHP metamorphic terrane of Dabieshan: chemical and isotopic constraints. *Lithos* 70, 243–267.
- Jahn, B.M., Rumble, D., Liou, J.G., 2003b. Geochemistry and isotope tracer study of UHP metamorphic rocks. *EMU Notes in Mineralogy* 5, 365–414.
- Krabbendam, M., Wain, A., Andersen, T.B., 2000. Pre-Caledonian granulite and gabbro enclaves in the Western Gneiss Region, Norway: indications of incomplete transition at high pressure. *Geological Magazine* 137, 235–255.
- Liou, J.G., Zhang, R.Y., 2002. Third ed. *Ultrahigh-pressure Metamorphic Rocks: Encyclopedia of Physical Sciences and Technology*, vol. 17. Academia Press, Tarzana, CA, pp. 227–244.
- Liou, J.G., Zhang, R.Y., Wang, X., Eide, E.A., Ernst, W.G., Maruyama, S., 1996. Metamorphism and tectonics of high-pressure and ultra-high-pressure belts in the Dabie–Sulu region, China. In: Yin, A., Harrison, T.M. (Eds.), *Tectonic Evolution of Asia*. Cambridge Univ. Press, Cambridge, pp. 300–344.
- Liou, J.G., Zhang, R.Y., Jahn, B.M., 1997. Petrology, geochemistry and isotope data on an ultrahigh-pressure jadeite quartzite from Shuanghe, Dabie Mountains, east-central China. *Lithos* 41, 59–78.
- Liou, J.G., Tsujimori, T., Zhang, R.Y., Katayama, I., Maruyama, S., 2004. Global UHP metamorphism and continental subduction/collision: the Himalayan model. *International Geology Review* 46, 1–27.
- Liu, L., Che, Z.C., Wang, Y., Luo, J.H., Chen, D.L., 1999. The petrological characters and geotectonic setting of high-pressure metamorphic rock belts in Altun Mountains. *Acta Petrologica Sinica* 15 (01), 57–64 (in Chinese with English abstract).
- Liu, L., Zhang, A.D., Chen, D.L., Yang, J.X., Luo, J.H., Wang, C., 2007. Implications based on LA-ICP-MS zircon U–Pb ages of eclogite and its country rock from Jianggalesayi area, Altyn Tagh. *Earth Science Frontiers* 14 (1), 98–107 (in Chinese with English abstract).
- Liu, Y.S., Gao, S., Jin, S.Y., Hu, S.H., Sun, M., Zhao, Z.B., Feng, J.L., 2001. Geochemistry and petrogenesis of lower crustal xenoliths from Hannuoba, North China: implications for the continental lower crustal composition and evolution at convergent margin. *Geochimica et Cosmochimica Acta* 65 (15), 2589–2604.
- Ludwig, K.R., 1997. Using Isoplot/EX, Version 2, in *A Geochronological Toolkit for Microsoft Excel*. Berkeley Geochronological Center Special Publication, Berkeley, p. 47.
- Ludwig, K.R., 2002. SQUID 1.02, a user's Manual. Berkeley Geochronology Center Special Publication 2, 2455 Ridge Road, Berkeley, CA 94709, USA, p. 22.
- Lugmair, G.W., Marti, K., 1978. Luna initial  $^{143}\text{Nd}/^{144}\text{Nd}$ : differential evolution of the lunar crust and mantle. *Earth and Planetary Science Letters* 39, 349–357.
- Malaspina, N., Hermann, J., Scambelluri, M., Compagnoni, R., 2006. Multi-stage metasomatism in ultrahigh-pressure mafic rocks from the North Dabie Complex (China). *Lithos* 90, 19–42.
- Maruyama, S., Liou, J.G., Terabayashi, M., 1996. Blueschists and eclogites of the world and their exhumation. *International Geology Review* 38, 485–594.
- Massonne, H.J., Schreyer, W., 1987. Phengite geobarometry based on the limitation assemblage with K-feldspar, phlogopite and Quartz. *Contributions to Mineralogy and Petrology* 96, 211–224.

- Mattinson, C.G., Wooden, J.L., Liou, J.G., Bird, D.K., Wu, C.L., 2006. Age and duration of eclogite-facies metamorphism, North Qaidam HP/UHP terrane, Western China. *American Journal of Science* 306, 683–711.
- Mattinson, C.G., Menold, C.A., Zhang, J.X., Bird, D.K., 2007. High- and ultrahigh-pressure Metamorphism in the North Qaidam and South Altyn Terranes, Western China. *International Geology Review* 49, 969–995.
- Meng, F.C., Zhang, J.X., Yang, J.S., Xu, Z.Q., 2003. Geochemical characteristics of eclogites in Xitieshan area, North Qaidam of northwestern China. *Acta Petrologica Sinica* 19, 435–442 (in Chinese with English abstract).
- Menold, C.A., Manning, C.E., Yin, A., Alex, R.C., Chen, X., 2002. Tectonic evolution of the North Qaidam UHP Complex, Western China. AGU Fall Meeting. Abstract# T51B-1159.
- Mercier, J.-C.C., 1980. Single-pyroxene thermobarometry. *Tectonophysics* 70, 1–37.
- Mével, C., 2003. Serpentinization of abyssal peridotites at mid-ocean ridges. *C.R. Geoscience* 335, 825–852.
- Morimoto, N., 1988. Nomenclature of pyroxenes. *American Mineralogist* 73, 1123–1133.
- Niu, Y.L., Batiza, R., 1997. Trace element evidence from seamounts for recycled oceanic crust in the eastern Pacific mantle. *Earth and Planetary Science Letters* 148, 471–483.
- Niu, Y.L., Hékinian, R., 1997a. Basaltic liquids and harzburgitic residues in the Garrett Transform: A case study at fast-spreading ridges. *Earth and Planetary Science Letters* 146, 243–258.
- Niu, Y.L., Hékinian, R., 1997b. Spreading-rate dependence of the extent of mantle melting beneath ocean ridges. *Nature* 385, 326–329.
- Niu, Y.L., 2005. Generation and evolution of basaltic magmas: some basic concepts and a hypothesis for the origin of the Mesozoic–Cenozoic volcanism in eastern China. *Geological Journal of China Universities* 11, 9–46.
- Niu, Y.L., Gilmore, T., Mackie, S., Greig, A., Bach, W., 2002. Mineral chemistry, whole-rock compositions and petrogenesis of ODP Leg 176 gabbros: data and discussion. In: Natland, J.H., Dick, H.J.B., Miller, D.J., Von Herzen, R.P. (Eds.), *Proc. ODP, Sci. Results*, vol. 176, pp. 1–60.
- O'Brien, P.J., 2001. Subduction followed by collision: Alpine and Himalayan examples. *Physics of the Earth and Planetary Interiors* 127, 277–291.
- Platt, J.P., 1986. Dynamics of orogenic wedges and the uplift of high-pressure metamorphic rocks. *Geological Society of America Bulletin* 97, 1037–1053.
- Ravna, E.J.K., Terry, M.P., 2004. Geothermobarometry of UHP and HP eclogites and schists — an evaluation of equilibria among garnet–clinopyroxene–kyanite–phengite–coesite/quartz. *Journal of Metamorphic Geology* 22, 579–592.
- Regenauer-Lieb, K., Yuen, D.A., Branlund, J., 2001. The initiation of subduction: criticality by addition of water? *Science* 294, 578–580.
- Reinecke, T., 1991. Very-high-pressure metamorphism and uplift of coesite-bearing metasediments from the Zermatt-Saas zone, Western Alps. *European Journal of Mineralogy* 3, 7–17.
- Rubatto, D., Gebauer, D., 2000. Use of cathodoluminescence for U–Pb zircon dating by ion microprobe: some examples from the Western Alps. In: Pagel, M., Barbi, V., Blanc, P., Ohnenstetter, D. (Eds.), *Cathodoluminescence in Geosciences*. Springer, Berlin Heidelberg New York, pp. 373–400.
- Rubatto, D., Gebauer, D., Fanning, M., 1998. Jurassic formation and Eocene subduction of the Zermatt-Saas-Fee ophiolites: implications for the geodynamic evolution of the Central and Western Alps. *Contribution to Mineralogy and Petrology* 132 (3), 269–287.
- Rubatto, D., Gebauer, D., Compagnoni, R., 1999. Dating of eclogite-facies zircons: the age of Alpine metamorphism in the Sesia-Lanzo Zone (Western Alps). *Earth and Planetary Science Letters* 167, 141–158.
- Scambelluri, M., Hoogerduijn Strring, E.H., Piccardo, G.B., Vissers, R.L.M., Rampone, E., 1991. Alpine olivine- and titanite-bearing assemblages in the Erro-Tobbio peridotite (Voltri Massif, NW Italy). *Journal of Metamorphic Geology* 9, 79–91.
- Scambelluri, M., Müntener, O., Hermann, J., Piccardo, G.B., Trommsdorff, V., 1995. Subduction of water into the mantle: history of and Alpine peridotite. *Geology* 23, 459–462.
- Song, S.G., 2001. Petrology, mineralogy and metamorphic evolution of the Dulan UHP Terrane in North Qaidam, NW China and its tectonic implications. Doctoral thesis in Institute of Geology, Chinese Academy of Geological Sciences.
- Song, S.G., Yang, J.S., Xu, Z.Q., Liou, J.G., Shi, R.D., 2003a. Metamorphic evolution of the coesite-bearing ultrahigh-pressure terrane in the North Qaidam, northern Tibet, NW China. *Journal of Metamorphic Geology* 21, 631–644.
- Song, S.G., Yang, J.S., Liou, J.G., Wu, C.L., Shi, R.D., Xu, Z.Q., 2003b. Petrology, geochemistry and isotopic ages of eclogites from the Dulan UHPM terrane, the North Qaidam, NW China. *Lithos* 70, 195–211.
- Song, S.G., Zhang, L.F., Niu, Y.L., 2004. Ultra-deep origin of garnet peridotite from the North Qaidam ultrahigh-pressure belt, Northern Tibetan Plateau, NW China. *American Mineralogist* 89, 1330–1336.
- Song, S.G., Zhang, L.F., Chen, J., Liou, J.G., Niu, Y., 2005a. Sodic amphibole exsolutions in garnet from garnet-peridotite, North Qaidam UHPM belt, NW China: implications for ultradeep-origin and hydroxyl defects in mantle garnets. *American Mineralogist* 90, 814–820.
- Song, S.G., Zhang, L.F., Su, L., Niu, Y.L., Song, B., 2005b. Geochronology of diamond-bearing zircons in garnet peridotite in the North Qaidam UHPM belt, North Tibetan Plateau: A record of complex histories associated with continental collision. *Earth and Planetary Science Letters* 234, 99–118.
- Song, S.G., Zhang, L.F., Niu, Y.L., Su, L., Song, B., Liu, D.Y., 2006. Evolution from oceanic subduction to continental collision: a case study of the Northern Tibetan Plateau inferred from geochemical and geochronological data. *Journal of Petrology* 47 (3), 435–455.
- Song, S.G., Su, L., Niu, Y., Zhang, L.F., 2007. Petrological and geochemical constraints on the origin of garnet peridotite in the North Qaidam ultrahigh-pressure Metamorphic Belt, Northwestern China. *Lithos* 96, 243–265.
- Spandler, C., Hermann, J., Arculus, R., Mavrogenes, J., 2004. Geochemical heterogeneity and element mobility in deeply subducted oceanic crust: insights from high-pressure mafic rocks from New Caledonia. *Chemical Geology* 206, 21–42.
- Steiger, R.H., Jager, E., 1977. Subcommittee on geochronology: convention of the use of decay constants in geo- and cosmochronology. *Earth Planetary Science Letters* 36, 359–362.
- Stern, R.A., 1998. High-resolution SIMS determination of radiogenic tracer-isotope ratios in minerals. In: Cabri, L.J., Vaughan, D.J. (Eds.), *Modern Approaches to Ore and Environmental Mineralogy*. Mineralogical Association of Canada, Short Course Series, vol. 27, pp. 241–268.
- Sun, S.S., McDonough, W.F., 1989. Chemical and isotopic systematics of oceanic basalt: implications for mantle composition and processes. In: Saunders, A.D., Norry, M.J. (Eds.), *Magmatism in the Ocean Basins*. Special Publication, vol. 42. Geological Society, London, pp. 313–345.
- Tilton, G.R., Schreyer, W., Schertl, H.P., 1991. Pb–Sr–Nd isotopic behavior of deeply subducted crustal rocks from the Dora Maira Massif, western Alps, Italy—II: what is the age of the ultrahigh-pressure metamorphism? *Contributions to Mineralogy and Petrology* 108, 22–33.
- Tilton, G.R., Ames, L., Schertl, H.-P., Schreyer, W., 1997. Reconnaissance isotopic investigations on rocks of an undeformed granite contact within the coesite-bearing unit of the Dora Maira Massif. *Lithos* 41, 25–36.
- Vavra, G., Gebauer, D., Schmid, R., Compston, W., 1996. Multiple zircon growth and recrystallization during polyphase Late Carboniferous to Triassic metamorphism in granulites of the Ivrea Zone (Southern Alps): an ion microprobe (SHRIMP) study. *Contributions to Mineralogy and Petrology* 122, 337–358.
- Von Quadt, A., Günther, D., Frischknecht, R., Zimmermann, R., Franz, G., 1997. The evolution of pre-Variscan eclogites of the Tauern Window (eastern Alps): A Sm/Nd, conventional and laser ICP-MS zircon U–Pb study. *Schweizerische Mineralogische und Petrographische Mitteilungen* 77, 265–279.
- Williams, I.S., 1998. U–Th–Pb geochronology by ion microprobe. In: McKibben, M.A., Shanks, W.C. (Eds.), *Applications of Microanalytical Techniques to Understanding Mineralizing Processes*. Reviews in Economic Geology, pp. 1–35.
- Witt-Eickchen, G., Seck, H.A., 1991. Solubility of Ca and Al in orthopyroxene from spinel peridotite: an improved version of an empirical geothermometer. *Contributions to Mineralogy and Petrology* 106, 431–439.
- Wunder, B., Schreyer, W., 1997. Antigorite: high-pressure stability in the system MgO–SiO<sub>2</sub>–H<sub>2</sub>O (MSH). *Lithos* 41, 213–227.
- Yang, J.J., Deng, J.F., 1994. Garnet peridotites and eclogites in the northern Qaidam Mountains, Tibetan plateau: a first record. First Workshop on UHP Metamorphism and Tectonics, ILP Task Group III-6. Stanford, A-20.

- Yang, J.J., Jahn, B.M., 2000. Deep subduction of mantle-derived garnet peridotites from the Su–Lu UHP metamorphic terrane in China. *Journal of Metamorphic Geology* 18, 167–180.
- Yang, J.S., Xu, Z.Q., Song, S.G., Zhang, J.X., Wu, C.L., Shi, R.D., Li, H.B., Maurice, B., 2001. Discovery of coesite in the North Qaidam Early Paleozoic ultrahigh pressure metamorphic belt, NW China. *Sciences De La Terre Et Des Planets* 333, 719–724.
- Yang, J.S., Zhang, J.X., Meng, F.C., Shi, R.D., Wu, C.L., Xu, Z.Q., Li, H.B., Chen, S.Y., 2003. Ultrahigh pressure eclogites of the north Qaidam and Altun mountains, NW China and their protoliths. *Earth Science Frontiers* 10, 291–314 (in Chinese with English abstract).
- Zhang, G.B., Song, S.G., Zhang, L.F., Niu, Y.L., Shu, G.M., 2005a. Ophiolite-type mantle peridotite from Shaliuhe, North Qaidam UHPM belt, NW China and its tectonic implications. *Acta Petrologica Sinica* 21 (4), 1049–1058 (in Chinese with English abstract).
- Zhang, J.X., Zhang, Z.M., Xu, Z.Q., Yang, J.S., Cui, J.W., 2001. Petrology and geochronology of eclogites from the western segment of the Altyn Tagh, northwestern China. *Lithos* 56, 189–208.
- Zhang, J.X., Yang, J.S., Mattinson, C.G., Xu, Z.Q., Meng, F.C., Shi, R.D., 2005b. Two contrasting eclogite cooling histories, North Qaidam HP/UHP terrane, western China: petrological and isotopic constraints. *Lithos* 84, 51–76.
- Zhang, L.F., Ellis, D.J., Jiang, W.B., 2002a. Ultrahigh pressure metamorphism in western Tianshan, China, part I: evidences from the inclusion of coesite pseudomorphs in garnet and quartz exsolution lamellae in omphacite in eclogites. *American Mineralogist* 87, 853–860.
- Zhang, L.F., Ellis, D., Williams, S., Jiang, W.B., 2002b. Ultrahigh pressure metamorphism in western Tianshan, China, part II: evidence from magnesite in eclogite. *American Mineralogist* 87, 861–866.
- Zhang, L.F., Ai, Y., Song, S., 2005c. The formation and tectonic evolution of UHP metamorphic belt in Southwestern Tianshan, Xinjiang. *Acta Petrologica Sinica* 21 (4), 1029–1037 (in Chinese with English abstract).
- Zhang, L.F., Ai, Y., Song, S., Song, B., Rubatto, D., Williams, S., Liou, J.G., Ellis, D., 2007. Triassic collision of Western Tianshan orogenic belt, China: evidences from SHRIMP U–Pb dating of zircon from eclogitic rocks, *Lithos*. *Lithos* 96, 266–280.
- Zhang, R.Y., Liou, J.G., Yang, J.S., 2000. Petrochemical constraints for dual origin of garnet peridotites of the Dabie–Sulu UHP terrane, China. *Journal of Metamorphic Geology* 18, 149–166.
- Zhang, R.Y., Zhai, S.M., Fei, Y.W., 2003. Titanium solubility in coexisting garnet and clinopyroxene at very high pressure: the significance of exsolved rutile in garnet. *Earth and Planetary Science Letters* 216, 591–601.
- Zheng, Y.F., Fu, B., Gong, B., Li, L., 2003. Stable isotope geochemistry of ultrahigh-pressure metamorphic rocks from the Dabie–Sulu orogen in China: implications for geodynamics and fluid regime. *Earth Science Review* 62, 105–161.